

Two-way Homogeneity Pursuit for Quantile Network Vector Autoregression

Wenyang Liu,^{1,†} Ganggang Xu,^{2,†} Jianqing Fan,^{3,*} and Xuening Zhu^{1,*}

¹*Fudan University, China,* ²*University of Miami, United States of America and*

³*Princeton University, United States of America.*

[†]*Wenyang Liu and Ganggang Xu are joint first authors. *Jianqing Fan and Xuening*

Zhu are joint corresponding authors. jqfan@princeton.edu (J. Fan);

xueningzhu@fudan.edu.cn (X. Zhu).

Abstract

While the Vector Autoregression (VAR) model has received extensive attention for modelling complex time series, quantile VAR analysis remains relatively underexplored for high-dimensional time series data. To address this disparity, we introduce a two-way grouped network quantile (TGNQ) autoregression model for time series collected on large-scale networks, known for their significant heterogeneous and directional interactions among nodes. Our proposed model simultaneously conducts node clustering and model estimation to balance complexity and interpretability. To account for the directional influence among network nodes, each network node is assigned two latent group memberships that can be consistently estimated using our proposed estimation procedure. Theoretical analysis demonstrates the consistency of membership and parameter estimators even with an overspecified number of groups. With the correct group specification, estimated parameters are proven to be asymptotically normal, enabling valid statistical inferences. Moreover, we propose a quantile information criterion for consistently selecting the number of groups. Simulation studies show promising finite sample performance, and we apply the methodology to analyze connectedness and risk spillover effects among Chinese A-share stocks.

KEY WORDS: Network data, Quantile vector autoregression, Two-way group structure, Two-way homogeneity pursuit.

1 Introduction

Quantile regression (Koenker and Bassett, 1978) is an important statistical tool for modeling associations between the response variable and covariates across different quantiles, which serves as a significant alternative to traditional conditional mean regression models. Its applicability spans various domains such as economic growth studies (Zhang et al., 2019; Chen et al., 2021), financial risk management (Diebold and Yilmaz, 2014; Härdle et al., 2016; Zhu et al., 2023a), air pollution assessments (Chen and Tokdar, 2021), and beyond.

Recently, there has been a notable surge in interest in applying quantile regression to panel data. To name a few, the panel quantile regression models with fixed or random effects are considered by Lamarche (2010) and Abrevaya and Dahl (2008). Kato et al. (2012) establish an asymptotic framework for theoretical analysis of the panel quantile regression model. Galvao and Kato (2016) develop a smoothed quantile regression loss which facilitates a novel theoretical analysis framework, which is further employed in Chen et al. (2021) and He et al. (2023) for valid inference and fast computation in complex quantile regression models. However, it is worth noting that most existing works assume cross-sectional independence among individuals.

With scarce attempts to address the issue, modeling heterogeneity among individuals in a quantile vector autoregressive model remains a significant challenge. For instance, in the quantile autoregression model proposed by Zhu et al. (2019b) and the dynamic network quantile regression model proposed by Xu et al. (2022), they both employ a set of common regression coefficients for all individuals in the systems. Ignoring such potential heterogeneity among individuals may result in model misspecification. Conversely, Ando et al. (2023) consider an individual-specific spatial effect,

necessitating the estimation of a large number of parameters, especially for a large-scale network, thereby leading to lower estimation efficiency.

To strike a balance between the model flexibility and estimation efficiency, a popular approach is to introduce group patterns among model coefficients. For instance, [Ke et al. \(2015\)](#) develop a homogeneity pursuit approach for discovering clustered pattern among the model coefficients. The group identification technique is also widely used for various panel data models to pursue homogeneity patterns among the individuals; see [Bonhomme and Manresa \(2015\)](#), [Bester and Hansen \(2016\)](#), [Su et al. \(2016\)](#), [Liu et al. \(2020\)](#) for relevant literature. Notably, for quantile regression models, the group structure is also introduced in recent literature to capture the potential heterogeneity pattern at different quantile levels. For example, [Zhang et al. \(2019\)](#) develop a quantile regression-based clustering procedure for identifying the subgroups of units in panel data. [Gu and Volgushev \(2019\)](#) utilize a penalized estimation approach to discover the group structure imposed on the fixed effects of quantile panel models. [Zhang et al. \(2023\)](#) propose a nonparametric quantile regression method for homogeneity pursuit in panel data models. However, they all assume independence among individuals and thus lack the ability to characterize the potential cross-sectional dependence structure.

To model the cross-sectional dependence, we utilize the network relationship collected among the individuals and embed it in a quantile autoregression framework. In terms of modelling the network dependence, the existing works in quantile autoregressive models often overlook the commonly observed directional influences among individuals in a network. However, we find that recent literature on community detection has highlighted that network nodes in different communities play distinct roles and have varying degrees of influence on other network communities ([Choi and Wolfe, 2014](#); [Rohe et al., 2016](#); [Ji and Jin, 2016](#); [Abbe et al., 2020, 2022](#); [Ke and Jin, 2023](#)).

For example, [Rohe et al. \(2016\)](#) classified communities as “sending communities” and “receiving communities” when designing a bi-clustering algorithm for directional networks. Acknowledging the importance of directional influence, our work proposes a two-way group structure to characterize better the distinct roles played by each network group in “influencing” and “receiving” influence from other network groups. This is a distinctive feature compared to the one-way group structure proposed in [Zhu et al. \(2023b\)](#), where each network node can only possess one group identity. We wish to emphasize that compared to the one-way group structure, introducing the two-way structure poses significant computational and theoretical challenges.

In this work, we propose a two-way grouped network quantile (TGNQ) autoregressive model, where each network node is characterized by two latent group memberships to capture directional influence among different groups. By assuming that group memberships are shared across different quantiles, we can simultaneously identify memberships and estimate parameters at multiple quantile levels. We introduce an efficient algorithm for solving the highly non-convex loss function and establish asymptotic properties of resulting estimators. Specifically, we derive clustering error rates and convergence rates of parameter estimators under the assumption of overspecified group numbers. Additionally, we develop a data-driven criterion for selecting the true group numbers with a probability approaching one. Given the correct identification of group numbers, we establish the asymptotic normality of estimated parameters at multiple quantile levels.

The rest of the paper is organized as follows. [Section 2](#) provides a comprehensive overview of the proposed method, detailing model specifications and the computational algorithm. Following this, [Section 3](#) examines the theoretical properties of the proposed method, including estimation consistency and a method for consistently selecting group

numbers. In Section 4, we establish the asymptotic normality of parameter estimators under the correct group number specification. Subsequently, Section 5 presents Monte Carlo simulations to evaluate the finite sample performance, while Section 6 applies the method to real-world data. The supplementary material provides additional details of the proposed algorithm, technical proofs, and supplementary experimental results.

2 Homogeneity Pursuit with Group Structures

2.1 Model and Notations

Consider a network represented by an adjacency matrix $\mathbf{A} = (a_{ij}) \in \{0, 1\}^{N \times N}$, where $a_{ij} = 1$ if an edge exists from the i th node to the j th node and 0 otherwise. Denote by $\mathcal{N}_i = \{j : a_{ij} \neq 0\}$ as the neighbouring set of node i , and by $n_i = |\mathcal{N}_i| = \sum_{j=1}^N a_{ij}$ as the out-degree of node i . The row-normalized weighting matrix is then given by $\mathbf{W} = (w_{ij})$, where $w_{ij} = a_{ij}/n_i$. For each node, we observe a time series of continuous variables, denoted by $\{Y_{it}, 0 \leq t \leq T\}$ for $1 \leq i \leq N$. Correspondingly, for each node, we collect a set of exogenous variables $\{\mathbf{x}_{it} \in \mathbb{R}^p : 1 \leq t \leq T\}$, where the dimension p is fixed. Denote the conditional quantile of Y_{it} as $Q_{it}(\tau|\mathcal{F}_{t-1})$, where \mathcal{F}_{t-1} is the σ -field generated by $\{(Y_{js}, \mathbf{x}_{j(s+1)}) : s \leq t-1, 1 \leq j \leq N\}$. Denote by $\boldsymbol{\tau}_K = \{\tau_1, \dots, \tau_K\}$ a set of pre-specified quantiles, and we consider the following two-way grouped network quantile (TGNQ) autoregression model at the τ th quantile

$$Q_{it}(\tau|\mathcal{F}_{t-1}) = \sum_{j=1}^N \theta_{g_i h_j}(\tau) w_{ij} Y_{j(t-1)} + \nu_{g_i}(\tau) Y_{i(t-1)} + \mathbf{x}_{it}^\top \boldsymbol{\gamma}_{g_i}(\tau), \quad \tau \in \boldsymbol{\tau}_K, \quad (2.1)$$

for any $1 \leq i \leq N$, where g_i and h_j are group memberships in the row and column, respectively. In (2.1), we express the conditional quantile in a linear form of three terms.

The first term represents a weighted average influence received from the following nodes in the previous time point. Particularly, $\theta_{g_i h_j}(\tau)$ quantifies the network effect from the j th node to the i th node at the τ th quantile, which is homogeneous within a two-way group membership (g_i, h_j) . Consequently, g_i represents the “receiving” group (referred to as the row group) membership of node i , and h_j represents the “influencing” group (referred to as the column group) membership of node j . On the group level, $\theta_{gh}(\tau)$ reflects the influence received by a member of the “receiving” group g and a member from the “influencing” group h , with $g \in [G]$ and $h \in [H]$. Subsequently, $\nu_{g_i}(\tau)$ quantifies the autoregressive effect in the previous time point from the same node and $\gamma_{g_i}(\tau)$ is the corresponding covariate effect.

Remark 1. *We remark that the heterogenous network effects have been noticed and modeled in recent literature. For instance, [Dou et al. \(2016\)](#) characterizes the receiving network effects with different coefficients for each node i . This can be achieved by ignoring the column group in our model framework. [Zhu et al. \(2019a\)](#) model the influential power of each node j with a regression coefficient associated with each node, and they identify important network nodes by a screening procedure. Similarly, within our framework, the influential power of node j can also be characterized by setting $\theta_{g_i h_j}(\tau)$ to $\theta_{h_j}(\tau)$. A bi-directional network influence modeling framework with a network regression model is proposed by [Wu et al. \(2022\)](#), where they encode the network effect further by using a functional transformation of the nodes’ covariates. Similar network autoregression models with one-way group structures are considered by [Zhu et al. \(2023b\)](#) and [Fang et al. \(2023\)](#) respectively, while they force the row and column group memberships to be identical.*

Denote by $\mathbf{y}_t = (Y_{1t}, \dots, Y_{Nt})^\top$ and model (2.1) can be re-written as follows

$$Y_{it} = \mathbf{b}_i(\tau)^\top \mathbf{y}_{t-1} + \mathbf{x}_{it}^\top \boldsymbol{\gamma}_{g_i}(\tau) + \varepsilon_{it}(\tau), \quad \tau \in \boldsymbol{\tau}_K,$$

where $\mathbf{b}_i(\tau) = (w_{ij}\theta_{g_i h_j}(\tau) : j \in [N])^\top + \mathbf{e}_i^{(N)} \nu_{g_i}(\tau) \in \mathbb{R}^N$ with $\mathbf{e}_i^{(N)}$ being an N -dimensional unit vector with the i th element being one and the others being zero. Here we define $\varepsilon_{it}(\tau) = Y_{it} - \mathbf{b}_i(\tau)^\top \mathbf{y}_{t-1} - \mathbf{x}_{it}^\top \boldsymbol{\gamma}_{g_i}(\tau)$ for which it holds that $P(\varepsilon_{it}(\tau) < 0 | \mathcal{F}_{t-1}) = \tau$. Consequently, the above model can be re-organized into the matrix form

$$\mathbf{y}_t = \mathbf{B}(\tau) \mathbf{y}_{t-1} + \boldsymbol{\mu}_{x,t}(\tau) + \boldsymbol{\varepsilon}_t(\tau), \quad \tau \in \boldsymbol{\tau}_K, \quad (2.2)$$

where $\mathbf{B}(\tau) = (\mathbf{b}_i(\tau) : 1 \leq i \leq N)^\top \in \mathbb{R}^{N \times N}$, $\boldsymbol{\mu}_{x,t}(\tau) = (\mathbf{x}_{it}^\top \boldsymbol{\gamma}_{g_i}(\tau) : 1 \leq i \leq N)^\top \in \mathbb{R}^N$, and $\boldsymbol{\varepsilon}_t(\tau) = (\varepsilon_{it}(\tau) : 1 \leq i \leq N)^\top \in \mathbb{R}^N$.

The proposed TGNQ model takes a vector autoregressive form (2.2) with a structured transition matrix $\mathbf{B}(\tau)$, which can be expressed as follows

$$\mathbf{B}(\tau) = \mathbf{W} \circ \boldsymbol{\Theta}(\tau) + \boldsymbol{\nu}(\tau), \quad \tau \in \boldsymbol{\tau}_K,$$

where \circ denotes the Hadamard product, $\boldsymbol{\Theta}(\tau) = (\theta_{g_i h_j}(\tau) : i, j \in [N]) \in \mathbb{R}^{N \times N}$ represents the matrix of interactions, and $\boldsymbol{\nu}(\tau) = \text{diag}\{\nu_{g_1}(\tau), \dots, \nu_{g_N}(\tau)\}$. It is worth noting that by performing row and column permutations, it's possible to rearrange the rows and columns of $\boldsymbol{\Theta}(\tau)$ such that entries with the same group memberships are grouped together. Consequently, the permuted version of $\boldsymbol{\Theta}(\tau)$ exhibits a block matrix structure with “rectangle-shaped” blocks. See Figure 1 for an illustration.

From Figure 1, we can interpret the proposed model (2.2) as follows: if the network is fully connected, the transition matrix $\mathbf{B}(\tau)$ can be permuted into a block matrix

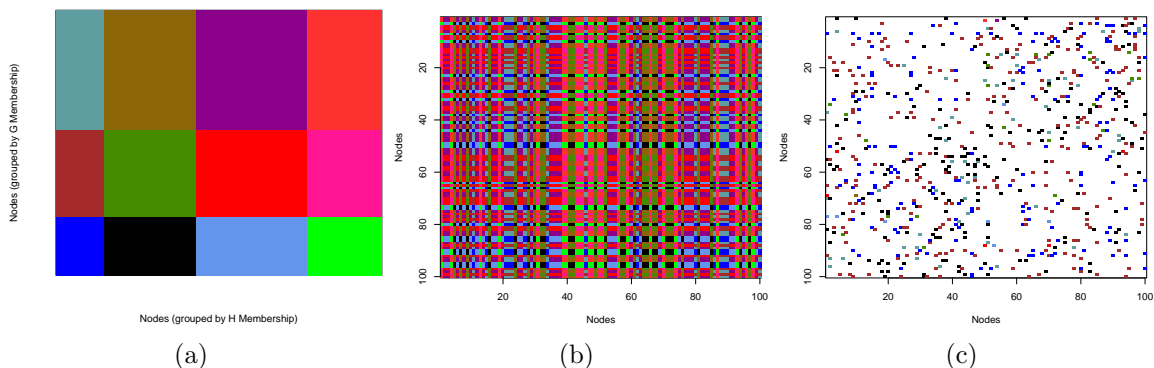


Figure 1: A simulated example with $N = 100$ nodes and $G = 3$ and $H = 4$ groups, respectively. (a) Row and column permuted $\Theta(\tau)$; (b) The original $\Theta(\tau)$; (c) Network sparsified $\Theta(\tau)$ (i.e., $\mathbf{W} \circ \Theta(\tau)$).

(except for the diagonal elements), which can be recovered by identifying the two-way group memberships. This process can be seen as a two-dimensional extension of the homogeneity pursuit approach (Ke et al., 2015) to the VAR model. However, in practice, it is unrealistic for a network to be fully connected. Therefore, the interactions between nodes in the VAR model are further sparsified by imposing a network structure, leading to a sparse $\mathbf{B}(\tau)$. Let $\mathbb{G} = (g_1, \dots, g_N)^\top$ and $\mathbb{H} = (h_1, \dots, h_N)^\top$ denote the membership vectors for the row and column groups respectively. To better understand the proposed model, we can further consider the following two special cases of the network effects $\theta_{g_i h_j}(\tau)$.

The additive network effects. We can further assume an additive form $\theta_{g_i h_j}(\tau) = \alpha_{g_i}(\tau) + \beta_{h_j}(\tau)$, and thus the transition matrix $\mathbf{B}(\tau)$ can be written as

$$\mathbf{B}(\tau) = \mathcal{A}_{\mathbb{G}}(\tau)\mathbf{W} + \mathbf{W}\mathcal{B}_{\mathbb{H}}(\tau) + \mathcal{V}_{\mathbb{G}}(\tau), \quad \tau \in \tau_K, \quad (2.3)$$

where $\mathcal{A}_{\mathbb{G}}(\tau) = \text{diag}\{\alpha_{g_1}(\tau), \dots, \alpha_{g_N}(\tau)\}$, $\mathcal{B}_{\mathbb{H}}(\tau) = \text{diag}\{\beta_{h_1}(\tau), \dots, \beta_{h_N}(\tau)\}$, and $\mathcal{V}_{\mathbb{G}}(\tau) = \text{diag}\{\nu_{g_1}(\tau), \dots, \nu_{g_N}(\tau)\}$.

Multiplicative network effects. We can also assume that $\theta_{g_i h_j}(\tau) = \alpha_{g_i}(\tau) \times \beta_{h_j}(\tau)$,

and thus express $\mathbf{B}(\tau)$ as

$$\mathbf{B}(\tau) = \mathcal{A}_{\mathbb{G}}(\tau)\mathbf{W}\mathcal{B}_{\mathbb{H}}(\tau) + \mathcal{V}_{\mathbb{G}}(\tau), \quad \tau \in \boldsymbol{\tau}_K. \quad (2.4)$$

In either case, the interaction between node i and node j , i.e., $\theta_{g_i h_j}(\tau)$, can be viewed as the joint effect of the “receptiveness” of node i , i.e., $\alpha_{g_i}(\tau)$, and the “influential power” of node j , i.e., $\beta_{h_j}(\tau)$. Such additional assumptions improve the interpretability of the proposed TGNQ model and are applicable in many scenarios.

2.2 Model Estimation

Let $\boldsymbol{\theta} = (\theta_{gh}(\tau_k) : g \in [G], h \in [H], 1 \leq k \leq K)^\top \in \mathbb{R}^{KGH}$, $\boldsymbol{\nu} = (\nu_g(\tau_k) : g \in [G], 1 \leq k \leq K)^\top \in \mathbb{R}^{KG}$, and $\boldsymbol{\gamma} = (\gamma_g(\tau_k)^\top : g \in [G], 1 \leq k \leq K)^\top \in \mathbb{R}^{KGp}$ collect all model parameters for pre-specified group numbers G and H . For convenience, we denote $\boldsymbol{\psi} = \{\boldsymbol{\theta}, \boldsymbol{\nu}, \boldsymbol{\gamma}\}$. Recall that $\mathbb{G} = (g_i : i \in [N])^\top$ and $\mathbb{H} = (h_j : j \in [N])^\top$ are the row and the column group membership vectors, respectively. Subsequently, the unknown parameters and memberships can be estimated by $(\widehat{\boldsymbol{\psi}}, \widehat{\mathbb{G}}, \widehat{\mathbb{H}})$, which minimizes the following multiple quantile loss function

$$\begin{aligned} \mathcal{L}(\boldsymbol{\psi}, \mathbb{G}, \mathbb{H}) &\stackrel{\text{def}}{=} \frac{1}{K} \sum_{k=1}^K \mathcal{L}_{\tau_k}(\boldsymbol{\psi}, \mathbb{G}, \mathbb{H}) \\ &\stackrel{\text{def}}{=} \frac{1}{NTK} \sum_{k=1}^K \sum_{i=1}^N \sum_{t=1}^T \rho_{\tau_k} \left(Y_{it} - \sum_{j=1}^N \theta_{g_i h_j}(\tau_k) w_{ij} Y_{j(t-1)} - \nu_{g_i}(\tau_k) Y_{i(t-1)} - \mathbf{x}_{it}^\top \boldsymbol{\gamma}_{g_i}(\tau_k) \right), \end{aligned} \quad (2.5)$$

where $\rho_\tau(u) = u\{\tau - I(u < 0)\}$ is the check function for the τ th quantile. With unknown \mathbb{G} and \mathbb{H} , the loss function (2.5) is highly nonconvex, rendering its minimization a challenging mixed integer optimization problem. To address this challenge, we have

devised the following algorithms.

2.2.1 The Vanilla Algorithm

We begin by introducing a simple algorithm that iteratively updates the model parameters and group memberships through coordinate descent. Let $\mathcal{R}_g = \{i : g_i = g\}$ and $\mathcal{C}_h = \{j : h_j = h\}$ for $g \in [G]$, $h \in [H]$. Define $\mathbf{y}_t^g = (Y_{it} : i \in \mathcal{R}_g)^\top \in \mathbb{R}^{|\mathcal{R}_g|}$, $\bar{\mathbf{y}}_t^{(g,h)} = (\sum_{j \in \mathcal{C}_h} w_{ij} Y_{jt} : i \in \mathcal{R}_g)^\top \in \mathbb{R}^{|\mathcal{R}_g|}$, and $Q_{\mathbf{y}_t^g}(\tau_k | \mathcal{F}_{t-1}) = \{Q_{it}(\tau_k | \mathcal{F}_{t-1}) : i \in \mathcal{R}_g\}^\top \in \mathbb{R}^{|\mathcal{R}_g|}$ as the τ_k th quantile vector for \mathbf{y}_t^g . Then, model (2.1) can be written as

$$Q_{\mathbf{y}_t^g}(\tau_k | \mathcal{F}_{t-1}) = \sum_h \bar{\mathbf{y}}_{t-1}^{(g,h)} \theta_{gh}(\tau_k) + \nu_g(\tau_k) \mathbf{y}_{t-1}^g + \mathbf{X}_t^g \boldsymbol{\gamma}_g(\tau_k) \stackrel{\text{def}}{=} \mathbf{Z}_{t-1}^g \boldsymbol{\xi}_g(\tau_k), \quad (2.6)$$

where $\mathbf{X}_t^g = (\mathbf{x}_{it} : i \in \mathcal{R}_g)^\top \in \mathbb{R}^{|\mathcal{R}_g| \times p}$, and $\mathbf{Z}_{t-1}^g = (\bar{\mathbf{Z}}_{t-1}^g, \mathbf{y}_{t-1}^g, \mathbf{X}_t^g) \in \mathbb{R}^{|\mathcal{R}_g| \times (H+p+1)}$ with $\bar{\mathbf{Z}}_{t-1}^g = (\bar{\mathbf{y}}_{t-1}^{(g,h)} : h \in [H]) \in \mathbb{R}^{|\mathcal{R}_g| \times H}$, and the parameter vector $\boldsymbol{\xi}_g(\tau_k) = (\theta_{g1}(\tau_k), \theta_{g2}(\tau_k), \dots, \theta_{gH}(\tau_k), \nu_g(\tau_k), \boldsymbol{\gamma}_g^\top(\tau_k))^\top \in \mathbb{R}^{H+p+1}$.

Utilizing the provided notations, Algorithm 1 outlines the vanilla algorithm for estimating the general TGNQ model (2.1). However, the estimation procedures for the additive model (2.3) and the multiplicative model (2.4) differ slightly from Algorithm 1, as we can further exploit their distinct structures. Detailed explanations are provided in Section A.2.1 of the supplementary material.

2.2.2 The Enhanced Algorithm

The Vanilla Algorithm 1 mirrors the algorithm employed in [Zhu et al. \(2023b\)](#), which proves particularly effective when each node assumes only one group membership. However, our empirical observations reveal that this method encounters difficulty in accurately determining the column membership \mathbb{H} because the coordinate descent al-

Algorithm 1 The Vanilla Algorithm

Denote $\widehat{\boldsymbol{\psi}}^{(l)}$, $\widehat{\mathbb{G}}^{(l)}$ and $\widehat{\mathbb{H}}^{(l)}$ as the estimators obtained after the l th iteration.

Step I: fix $\mathbb{G} = \widehat{\mathbb{G}}^{(l)}$ and $\mathbb{H} = \widehat{\mathbb{H}}^{(l)}$, update $\widehat{\boldsymbol{\psi}}^{(l)}$ by $\widehat{\boldsymbol{\psi}}^{(l+1)}$, whose components are estimated as $\widehat{\boldsymbol{\xi}}_g^{(l+1)}(\tau_k) = \arg \min_{\boldsymbol{\xi}_g} \sum_{t=1}^T \sum_{i \in \mathcal{R}_g} \rho_{\tau_k}(Y_{it} - \mathbf{z}_{i,t-1}^{g\top} \boldsymbol{\xi}_g)$ for $g \in [G]$, $\tau_k \in \boldsymbol{\tau}_K$, where $\mathbf{z}_{i,t-1}^{g\top}$ is the i th row of \mathbf{Z}_{t-1}^g .

Step II: fix $\boldsymbol{\psi} = \widehat{\boldsymbol{\psi}}^{(l+1)}$ and $\mathbb{H} = \widehat{\mathbb{H}}^{(l)}$, update $\widehat{\mathbb{G}}^{(l)}$ by $\widehat{\mathbb{G}}^{(l+1)} = (\widehat{g}_1^{(l+1)}, \dots, \widehat{g}_N^{(l+1)})^\top$, where $\widehat{g}_i^{(l+1)}$ minimizes the following loss function (with respect to g_i):

$$\sum_{k=1}^K \sum_{t=1}^T \rho_{\tau_k} \left\{ Y_{it} - \sum_{j=1}^N \widehat{\theta}_{g_i \widehat{h}_j^{(l)}}^{(l+1)}(\tau_k) w_{ij} Y_{j(t-1)} - \widehat{v}_{g_i}^{(l+1)}(\tau_k) Y_{i(t-1)} - \mathbf{x}_{it}^\top \widehat{\boldsymbol{\gamma}}_{g_i}^{(l+1)}(\tau_k) \right\}.$$

Step III: fix $\boldsymbol{\psi} = \widehat{\boldsymbol{\psi}}^{(l+1)}$ and $\mathbb{G} = \widehat{\mathbb{G}}^{(l+1)}$, update $\widehat{\mathbb{H}}^{(l)}$ by $\widehat{\mathbb{H}}^{(l+1)} = (\widehat{h}_1^{(l+1)}, \dots, \widehat{h}_N^{(l+1)})^\top$, where $\widehat{h}_j^{(l+1)}$ minimizes the following loss function (with respect to h_j):

$$\begin{aligned} \sum_{k=1}^K \sum_{i=1}^N \sum_{t=1}^T \rho_{\tau_k} \left(Y_{it} - \sum_{j': j' \neq j}^N \widehat{\theta}_{\widehat{g}_i^{(l+1)} \widetilde{h}_{j'}}^{(l+1)}(\tau_k) w_{ij'} Y_{j'(t-1)} \right. \\ \left. - \widehat{\theta}_{\widehat{g}_i^{(l+1)} h_j}^{(l+1)}(\tau_k) w_{ij} Y_{j(t-1)} - \widehat{v}_{\widehat{g}_i^{(l+1)}}^{(l+1)}(\tau_k) Y_{i(t-1)} - \mathbf{x}_{it}^\top \widehat{\boldsymbol{\gamma}}_{\widehat{g}_i^{(l+1)}}^{(l+1)}(\tau_k) \right), \end{aligned}$$

where $\widetilde{h}_{j'} = \widehat{h}_{j'}^{(l+1)}$ if $j' < j$ and $\widetilde{h}_{j'} = \widehat{h}_{j'}^{(l)}$ if $j' > j$. Repeat Step III for several rounds until no $\widehat{h}_j^{(l+1)}$ can be changed.

Repeat Steps I-III until the algorithm converges.

gorithm often gets trapped in local minima. To tackle this challenge, we propose an enhanced algorithm specifically tailored to facilitate escaping local minima while estimating \mathbb{H} .

After obtaining $\widehat{\boldsymbol{\psi}}$, $\widehat{\mathbb{G}}$, and $\widehat{\mathbb{H}}$ from Algorithm 1, we continue to find a good set of proposals for \mathbb{H} to escape the possible local minima $\widehat{\mathbb{H}}$ by dividing the nodes into two sets: the active sets \mathcal{A} and the inactive set \mathcal{A}^c . If $j \in \mathcal{A}^c$, then \widehat{h}_j is considered reliable and need not be updated. In the beginning, we let the active set $\mathcal{A}_{(0)} = \{1, \dots, N\}$.

Next, in the r th round ($r = 1, 2, \dots$), we calculate the following

$$(\tilde{h}_{ij} : j \in \mathcal{A}_{(r-1)} \cap \mathcal{N}_i) = \underset{(h_j : j \in \mathcal{A}_{(r-1)} \cap \mathcal{N}_i)}{\operatorname{argmin}} \sum_{k=1}^K \sum_{t=1}^T \rho_{\tau_k} \left(r_{it}(\tau_k) - \sum_{j \in \mathcal{A}_{(r-1)} \cap \mathcal{N}_i} \hat{\theta}_{\hat{g}_i h_j}(\tau_k) w_{ij} Y_{j(t-1)} \right), \quad (2.7)$$

for each $1 \leq i \leq N$, where $r_{it}(\tau_k) = Y_{it} - \sum_{j \in \mathcal{A}_{(r-1)}^c \cap \mathcal{N}_i} \hat{\theta}_{\hat{g}_i \hat{h}_j}(\tau_k) w_{ij} Y_{j(t-1)} - \hat{\nu}_{\hat{g}_i}(\tau_k) Y_{i(t-1)} - \mathbf{x}_{it}^\top \hat{\gamma}_{\hat{g}_i}(\tau_k)$ and the estimators $\{\hat{\psi}, \hat{\mathbb{G}}\}$ are fixed. Given that the cardinality of $\mathcal{A}_{(r-1)} \cap \mathcal{N}_i$ is typically not large, solving the above minimization problem through enumeration is straightforward. However, in cases where $|\mathcal{A}_{(r-1)} \cap \mathcal{N}_i|$ is relatively large, we resort to using the discrete optimization routine provided by the R package **CEoptim** (Benham et al., 2017) to solve it. Then, we update an estimator $\tilde{\mathbb{H}}_{(r)} = (\tilde{h}_1, \dots, \tilde{h}_N)^\top$ for estimating \mathbb{H} based on the $\{\tilde{h}_{ij}\}$ obtained in (2.7). Specifically, for $j \in \mathcal{A}_{(r-1)}^c$, \tilde{h}_j is set to \hat{h}_j , while for $j \in \mathcal{A}_{(r-1)}$, \tilde{h}_j is randomly drawn from the vector $(\tilde{h}_{ij} : i \in \mathbb{F}_j)$, where $\mathbb{F}_j = \{i : a_{ij} = 1\}$ represents the set of followers for node j . When $\hat{\psi}$ and $\hat{\mathbb{G}}$ are close to the truth, one naturally expects that $\tilde{\mathbb{H}}$ should also be reasonably close to the truth. Therefore, if \tilde{h}_j coincides with \hat{h}_j for $j \in \mathcal{A}_{(r-1)}$, there would be more confidence in their accuracy, prompting the removal of node j from the active set. Consequently, we update the active set as $\mathcal{A}_{(r)} = \{j \in [N] : \hat{h}_j \neq \tilde{h}_j\}$.

Subsequently, we randomly partition the nodes in $\mathcal{A}_{(r)}$ into $\mathcal{A}_{(r,1)}$ and $\mathcal{A}_{(r,2)}$, and denote $\tilde{\mathbb{H}}_{(r,s)}$ ($s = 1, 2$) as the column membership vector by replacing \hat{h}_j with \tilde{h}_j for $j \in \mathcal{A}_{(r,s)}$ in $\hat{\mathbb{H}}$. Next, we check if $\tilde{\mathbb{H}}_{(r,s)}$ ($s = 1, 2$) can improve the objective function by using $\hat{\psi}$, $\hat{\mathbb{G}}$, and $\tilde{\mathbb{H}}_{(r,s)}$ as the initial inputs for Vanilla Algorithm 1. If the objective function fails to improve, we can resample $\tilde{\mathbb{H}}_{(r)}$ or update the active set $\mathcal{A}_{(r-1)}$ for more attempts until the algorithm converges. The specific iterative steps are summarized in Algorithm 2.

As the r increases in Step II of Algorithm 2, the active set $\mathcal{A}_{(r)}$ diminishes. This

Algorithm 2 The Enhanced Algorithm

Step I (INITIALIZATION) Set $r = 0$ and the active set $\mathcal{A}_{(0)} = \{1, \dots, N\}$. Run Algorithm 1 and denote the corresponding output as $\widehat{\boldsymbol{\psi}}_{(r)}$, $\widehat{\mathbb{G}}_{(r)}$ and $\widehat{\mathbb{H}}_{(r)}$. Repeat **Step II–IV**.

Step II (DRAW PROPOSALS FROM UPDATED ACTIVE SET) Obtain $\widetilde{h}_{ij}, i \in [N], j \in \mathcal{A}_{(r)} \cap \mathcal{N}_i$ using (2.7). Set $r = r + 1$.

- **If** $\widetilde{h}_{ij} = \widehat{h}_{(r)j}$ for all $i \neq j \in [N]$ **or** $r > r_{\max}$, **end** the algorithm and return $\{\widehat{\boldsymbol{\psi}}_{(r-1)}, \widehat{\mathbb{G}}_{(r-1)}, \widehat{\mathbb{H}}_{(r-1)}\}$.

Step III (IMPROVING THE OBJECTIVE FUNCTION)

(3.1) Obtain $\widetilde{\mathbb{H}}_{(r)}$ by randomly drawing \widetilde{h}_j for $j \in \mathcal{A}_{(r-1)}$ from the vector $(\widetilde{h}_{ij} : i \in \mathbb{F}_j)$ and update $\mathcal{A}_{(r)} = \{j : \widetilde{h}_j \neq \widehat{h}_{(r)j}\}$.

(3.2) Uniformly split $\mathcal{A}_{(r)}$ to obtain $\widetilde{\mathbb{H}}_{(r,1)}$ and $\widetilde{\mathbb{H}}_{(r,2)}$.

(3.3) Use $\widehat{\boldsymbol{\psi}}_{(r-1)}$, $\widehat{\mathbb{G}}_{(r-1)}$, and $\widetilde{\mathbb{H}}_{(r,s)}, s = 1, 2$ as the initial inputs for Algorithm 1.

(3.4) Repeat Steps (3.1)–(3.3). **If** the objective fails to improve for consecutive 10 times, go to **Step II**; **else** go to **Step I**.

Output $\{\widehat{\boldsymbol{\psi}}_{(r)}, \widehat{\mathbb{G}}_{(r)}, \widehat{\mathbb{H}}_{(r)}\}$.

suggests that the number of memberships in $\widehat{\mathbb{H}}$ requiring alteration decreases, thus potentially accelerating the convergence of the algorithm. Across all our numerical experiments, the enhanced Algorithm 2 demonstrates remarkable performance, consistently achieving accurate identification of true group memberships with high probability as T increases. However, providing theoretical justification for Algorithm 2 poses a significant challenge and remains an intriguing avenue for future research.

3 Theoretical Properties

In this section, we investigate the theoretical properties of the estimated parameters of the TGNQ model. Denote the true parameter as $\boldsymbol{\psi}^0 = \{\boldsymbol{\theta}^0, \boldsymbol{\nu}^0, \boldsymbol{\gamma}^0\}$. We first present a set of technical conditions in the following section.

3.1 Technical Conditions

To establish the theoretical properties, we require the following technical conditions.

Assumption 1. (CONDITIONAL DENSITY) *Assume that for each i , the stochastic process $\boldsymbol{\zeta}_{it} = (\mathbf{y}_{t,\mathcal{N}_i}^\top, \mathbf{x}_{it}^\top)^\top$, $t = 1, \dots, T$, is strictly stationary over t . Denote the conditional density of $\varepsilon_{it}(\tau)$ given $\boldsymbol{\zeta}_{it}$ as $f_{i,\tau}(u|\boldsymbol{\zeta}_{it})$, and we further assume that there exists a constant \bar{f} such that $\max_{i,k} \sup_{u,\boldsymbol{\zeta}} |f_{i,\tau_k}(u|\boldsymbol{\zeta})| < \bar{f}$ and $\max_{i,k} \sup_{u,\boldsymbol{\zeta}} |f'_{i,\tau_k}(u|\boldsymbol{\zeta})| < \bar{f}$, where $f'_{i,\tau_k}(u|\boldsymbol{\zeta})$ is the first order derivative of $f_{i,\tau_k}(u|\boldsymbol{\zeta})$.*

Assumption 2. (PARAMETER SPACE) *Assume $\max\{\|\boldsymbol{\theta}\|_{\max}, \|\boldsymbol{\nu}\|_{\max}, \|\boldsymbol{\gamma}\|_{\max}\} < c$, where c is a finite constant.*

Assumption 3. (MOMENT CONDITIONS) *Define the matrix $\boldsymbol{\Sigma}_i(\tau) = \mathbb{E}\{f_{i,\tau}(0|\boldsymbol{\zeta}_{it})\boldsymbol{\zeta}_{it}\boldsymbol{\zeta}_{it}^\top\}$. Assume that (a) $\max_{i,t} \sup_{\|\mathbf{u}\|=1} \mathbb{E}(|\boldsymbol{\zeta}_{it}^\top \mathbf{u}|^3) = O(1)$, (b) $\lambda_{\max}(\mathbb{E}(\boldsymbol{\zeta}_{it}\boldsymbol{\zeta}_{it}^\top)) \leq \sigma_{\max}$, and that (c) $\min_{i,k} \lambda_{\min}(\boldsymbol{\Sigma}_i(\tau_k)) \geq \sigma_{\min}$, where σ_{\min} and σ_{\max} are finite positive constants.*

Assumption 4. (GROUP DIFFERENCES) *Assume that (a) $\min_{g \neq g' \in [G_0]} \{K^{-1} \sum_{k=1}^K (|\nu_g^0(\tau_k) - \nu_{g'}^0(\tau_k)|^2 + \|\boldsymbol{\gamma}_g^0(\tau_k) - \boldsymbol{\gamma}_{g'}^0(\tau_k)\|^2)\} \geq c_0$; (b) $\min_{h_0 \neq h'_0 \in [H_0]} \sum_{g_0 \in [G_0]} (K^{-1} \sum_{k=1}^K |\theta_{g_0 h_0}^0(\tau_k) - \theta_{g_0 h'_0}^0(\tau_k)|^2) \geq c_0$, and (c) there exists a set $\mathcal{M}_H \subset [N]$ such that $|\mathcal{M}_H^c|/N \rightarrow 0$ and*

$$\min_{j \in \mathcal{M}_H} \min_{h \neq h'_j} \left\{ \frac{1}{K} \sum_{k=1}^K \sum_{i=1}^N w_{ij}^2 \left| \theta_{g_i^0 h_j^0}^0(\tau_k) - \theta_{g_i^0 h'_j}^0(\tau_k) \right|^2 \right\} \geq c_0, \quad (3.1)$$

where c_0 is a finite positive constant.

Assumption 5. (GROUP RATIOS AND NETWORK STRUCTURE) *Let $\pi_{g_0}^{(1)} = \sum_i I(g_i^0 = g_0)/N$, $\pi_{h_0}^{(2)} = \sum_j I(h_j^0 = h_0)/N$, and $\pi_{g_0 h_0} = N^{-1} \sum_{i,j} I(g_i^0 = g_0, h_j^0 = h_0) w_{ij}^2$. Assume that (a) $\min_{g_0 \in [G_0], h_0 \in [H_0]} \{\pi_{g_0}^{(1)}, \pi_{h_0}^{(2)}, \pi_{g_0 h_0}\} \geq c_\pi$, where c_π is a positive constant; (b) $N^{-1} \sum_j q_j^2 \leq c$, where $q_j = \sum_i w_{ij}^2$ and c is a positive constant.*

Assumption 6. (DISTRIBUTION CONDITIONS) Let $\mathbf{z}_t \stackrel{\text{def}}{=} (\mathbf{y}_t^\top, \mathbf{x}_{1t}^\top, \mathbf{x}_{2t}^\top, \dots, \mathbf{x}_{Nt}^\top)^\top$ and assume the following conditions hold. (a) The process $\{\mathbf{z}_t\}$ is geometrically β -mixing that there exist constants $c > 0$ and $\gamma_1 > 0$ such that $\beta(n) \leq 2 \exp(-cn^{\gamma_1})$ for any $n > 1$, where $\beta(n)$ denotes the β -mixing coefficient for the σ -fields associated with $\{\mathbf{z}_s : s \leq t\}$ and $\{\mathbf{z}_s : s \geq t + n\}$. (b) The random vector \mathbf{z}_t follows a sub-Weibull(γ_2) distribution in the sense that there exists a constant K_z such that $\|\mathbf{z}_t\|_{\phi_{\gamma_2}} \leq K_z < \infty$ for $t \in [T]$, where the sub-Weibull(γ) norm for a random variable X is defined as $\|X\|_{\phi_\gamma} = \sup_{p \geq 1} (\mathbb{E}|X|^p)^{1/p} p^{-1/\gamma}$ and $\|\mathbf{z}\|_{\phi_\gamma} = \sup_{\mathbf{v} \in \mathbb{R}^n, \|\mathbf{v}\|=1} \|\mathbf{v}^\top \mathbf{z}\|_{\phi_\gamma}$. (c) Let $\gamma = (\gamma_1^{-1} + \gamma_2^{-1})^{-1} < 1$ and $T^{\gamma_3} \gg n_{\max} \log(NK)$ with $\gamma_3 = (\gamma_1^{-1} + 3\gamma_2^{-1})^{-1}$, where $n_{\max} \stackrel{\text{def}}{=} \max_{i \in [N]} n_i$ represents the maximum out-degree of nodes.

We'd like to comment on the conditions as follows. Assumption 1 constitutes a regular condition by assuming stationarity of the time series and a uniformly upper bounded density function. The strict stationarity of generalized autoregressive processes is studied by Bougerol and Picard (1992), and such assumptions are commonly needed in quantile regression literature to ensure tractability and robustness of the loss function (Zhang et al., 2019; Chen et al., 2021; Ando et al., 2023). Assumption 2 assumes a bounded parameter space, while Assumption 3 imposes moment conditions on ζ_{it} and lower bounds on $\Sigma_i(\tau_k)$, ensuring local convexity of the loss function around the true parameters.

Assumptions 4 and 5 impose certain conditions on the group fractions and network connections, akin to those widely assumed in recent group panel data literature (Ando and Bai, 2016, 2017; Zhang et al., 2019; Liu et al., 2020; Zhu et al., 2023b; Fang et al., 2023). Assumption 4 essentially requires a constant gap between different groups at least at some considered quantile levels, ensuring distinguishability among groups. Assumption 4(a), applied to the row groups, resembles a similar condition in Liu et al.

(2020). Assumptions 4(b)-(c), applied to the column groups, involve the network structure and an index set \mathcal{M}_H , whose size controls the asymptotic clustering error of the \mathbb{H} memberships, as suggested by Theorem 2. Subsequently, Assumption 5 requires that the group ratios are lower bounded, ensuring that the group sizes diverge at the same rate as the network size N . Additionally, since we consider a two-way network structure, sufficient cross-group network edges (characterized by $\pi_{g_0 h_0}$) are needed to guarantee convergence of group interaction parameters. Lastly, the boundedness of $N^{-1} \sum_j q_j^2$ is assumed to facilitate our theoretical analysis for estimation consistency.

Assumption 6 assumes that the stochastic process \mathbf{z}_t is β -mixing over time and follows a sub-Weibull distribution. The β -mixing condition is relatively general and widely assumed in high-dimensional time series modelling literature (Fan and Yao, 2003; Zhang et al., 2019; Wang and Tsay, 2023). Additionally, the sub-Weibull distribution condition can be equivalently expressed as a tail condition, i.e., $P(\sup_{\|\mathbf{v}\|=1} |\mathbf{v}^\top \mathbf{z}_t| > u) \leq 2 \exp\{-(u/K_1)^{\gamma_2}\}$, where K_1 is a constant depending only on γ_2 (Wong et al., 2020). Thus, it includes sub-Gaussian and sub-exponential distributions as special cases and can also characterize heavy-tailed distributions by specifying $\gamma_2 < 1$ (Foss et al., 2011). Compared to the typical bounded condition imposed on regressors in quantile regression literature (Kato et al., 2012; Zhang et al., 2019), the sub-Weibull distribution assumption is more general. Lastly, Assumption 6 (c) specifies the relationship between γ_1 and γ_2 , under which concentration inequality can be obtained for β -mixing sequences, a condition also assumed in Wong et al. (2020).

3.2 Estimation Consistency When $G \geq G_0$ and $H \geq H_0$

We first establish the estimation consistency when the group numbers are possibly overspecified, i.e., $G \geq G_0$ and $H \geq H_0$. The following theorem provides the overall

convergence rate of all model parameters, including group memberships.

Theorem 1. *Assume Conditions 1–6, if $G \geq G_0$ and $H \geq H_0$, then we have that*

$$\begin{aligned} \frac{1}{NK} \sum_{i=1}^N \sum_{k=1}^K \left\{ \sum_{j \in \mathcal{N}_i} w_{ij}^2 |\hat{\theta}_{\hat{g}_i \hat{h}_j}(\tau_k) - \theta_{g_i^0 h_j^0}(\tau_k)|^2 + |\hat{\nu}_{\hat{g}_i}(\tau_k) - \nu_{g_i^0}(\tau_k)|^2 \right. \\ \left. + \|\hat{\gamma}_{\hat{g}_i}(\tau_k) - \gamma_{g_i^0}(\tau_k)\|^2 \right\} = O_p \left(\frac{\bar{n} \log(NK)}{T} \right), \end{aligned} \quad (3.2)$$

where $\bar{n} = N^{-1} \sum_i n_i$ represents the average out-degree of nodes.

The proof of Theorem 1 is given in Section A.3 of the supplementary material. By (3.2), the overall estimation error enjoys an $O_p(\bar{n} \log(NK)/T)$ convergence rate. This indicates that for a network with a large average network degree \bar{n} , the convergence becomes slower due to the potentially complex dependence structure.

Subsequently, based on (3.2), we can further proceed to obtain error bounds for the mis-clustering rates for both types of groups. To this end, define $\hat{\mathcal{R}}_g = \{i : \hat{g}_i = g\}$ and $\hat{\mathcal{C}}_h = \{j : \hat{h}_j = h\}$ as the set of estimated group members. To properly measure the clustering error, following Zhu et al. (2023b), we first define the following maps $\chi_1 : [G] \rightarrow [G_0]$ and $\chi_2 : [H] \rightarrow [H_0]$ as

$$\chi_1(g) = \arg \max_{g' \in [G_0]} \sum_i I(i \in \hat{\mathcal{R}}_g, g_i^0 = g'), g \in [G], \quad (3.3)$$

$$\chi_2(h) = \arg \max_{h' \in [H_0]} \sum_j I(j \in \hat{\mathcal{C}}_h, h_j^0 = h'), h \in [H]. \quad (3.4)$$

Here $\chi_1(g)$ and $\chi_2(h)$ map g and h to the true groups where most nodes in $\hat{\mathcal{R}}_g$ and $\hat{\mathcal{C}}_h$

belong. Based on this mapping, the membership estimation errors can be defined as

$$\hat{\varrho}_1 = \frac{1}{N} \sum_{g=1}^G \sum_{i=1}^N I \left(i \in \hat{\mathcal{R}}_g, g_i^0 \neq \chi_1(g) \right), \quad (3.5)$$

$$\hat{\varrho}_2 = \frac{1}{N} \sum_{h=1}^H \sum_{j=1}^N I \left(j \in \hat{\mathcal{C}}_h, h_j^0 \neq \chi_2(h) \right). \quad (3.6)$$

We remark that $1 - \hat{\varrho}_1$ and $1 - \hat{\varrho}_2$ are widely used in the machine learning literature and are commonly referred to as the clustering purity (Schütze et al., 2008). The error bounds for $\hat{\varrho}_1$ and $\hat{\varrho}_2$ are established in the next Theorem.

Theorem 2. *Assume Conditions 1–6, if $G \geq G_0$ and $H \geq H_0$, then we have $\hat{\varrho}_1 = O_p(\bar{n} \log(NK)/T)$ and $\hat{\varrho}_2 = O_p(\bar{n} \log(NK)/T + N^{-1}|\mathcal{M}_H^c|)$, where \mathcal{M}_H is given in Assumption 4.*

The proof of Theorem 2 is provided in Section A.4 of the supplementary material. The mis-clustering rate for the row group is $O_p(\bar{n} \log(NK)/T)$, suggesting that a larger T yields better clustering accuracy. This result is similar to those in Zhu et al. (2023b). However, the derivation of the clustering error bound for the column memberships is much more challenging and significantly different from proofs in the existing literature. In particular, we manage to show that the upper bound of $\hat{\varrho}_2$ is also controlled by the size of the identifiable node set defined by Assumption 4(c). In the special case where $\mathcal{M}_H = [N]$, we have $|\mathcal{M}_H^c| = 0$, and the mis-clustering rate $\hat{\varrho}_2$ converges at the same speed as $\hat{\varrho}_1$.

3.3 Group Number Identification

Note that the group numbers (G, H) are pre-specified when optimizing the objective function (2.5). The mis-specification of the group numbers may lead to unsat-

isfactory performance of the estimators. Therefore, it is crucial to develop a group number estimation procedure that can consistently estimate the true group numbers (G_0, H_0) . For pre-specified group numbers (G, H) , denote the corresponding estimators as $\widehat{\boldsymbol{\psi}}^{(G,H)}, \widehat{\mathbb{G}}^{(G,H)}, \widehat{\mathbb{H}}^{(G,H)}$ in this subsection by slightly abusing the notation. To select the number of row and column groups, we introduce the following quantile loss-based information criterion (QIC)

$$\text{QIC}_{\lambda_{NT}}(G, H) = \log\{\mathcal{L}(\widehat{\boldsymbol{\psi}}^{(G,H)}, \widehat{\mathbb{G}}^{(G,H)}, \widehat{\mathbb{H}}^{(G,H)})\} + \lambda_{NT}G(H + p + 1), \quad (3.7)$$

where λ_{NT} is a tuning parameter, and $G(H + p + 1)$ is the total number of model parameters. Then we can estimate G and H as $(\widehat{G}, \widehat{H}) = \arg \min_{G,H} \text{QIC}_{\lambda_{NT}}(G, H)$. In the following, we show that the group number can be consistently estimated when λ_{NT} is appropriately chosen.

Theorem 3. *Assume Conditions 1–6, then if $\lambda_{NT} \rightarrow 0$ and $\lambda_{NT}T/\{\bar{n} \log(NK)\} \rightarrow \infty$, we have that $P(\widehat{G} = G_0, \widehat{H} = H_0) \rightarrow 1$ as $(N, T) \rightarrow \infty$.*

The proof of Theorem 3 is provided in Section A.5 of the supplementary material. The tuning parameter λ_{NT} should converge to zero at a certain rate to ensure that the model is neither under-fitted nor overfitted. In our numerical study, we specify λ_{NT} as $N^{1/10}T^{-1} \log(T)/(10 \min \bar{n}, 10)$, yielding a good finite sample performance. Additionally, we note that establishing the consistency result for \widehat{H} is more challenging than for \widehat{G} . This is primarily because the clustering error for the \mathbb{G} memberships is inseparable from the theoretical analysis of \widehat{H} and requires careful attention.

4 Model Inference When $G = G_0$ and $H = H_0$

In this section we discuss the model inference based on the estimated TGNQ model under the assumption that $G = G_0$ and $H = H_0$. To establish a valid inference procedure, we first conduct membership refinements for $\widehat{\mathbb{G}}$ and $\widehat{\mathbb{H}}$ respectively, which are necessary to establish asymptotic normality of model parameter estimators.

4.1 Membership Refinement

4.1.1 Refinement of \mathbb{G} Membership

Denote by $\mathbb{H}_i = (h_j : j \in \mathcal{N}_i)^\top \in \mathbb{R}^{n_i}$ as the group memberships of nodes followed by the i th node. Let $\boldsymbol{\theta}_{g_i, \mathbb{H}_i}(\tau_k) = (\theta_{g_i h_j}(\tau_k) : j \in \mathcal{N}_i)^\top \in \mathbb{R}^{n_i}$, $\boldsymbol{\zeta}_{g_i}(\tau_k) = (\nu_{g_i}(\tau_k), \boldsymbol{\gamma}_{g_i}^\top(\tau_k))^\top \in \mathbb{R}^{p+1}$ and correspondingly the concatenated parameter vectors as $\boldsymbol{\theta}_{g_i, \mathbb{H}_i} = (\boldsymbol{\theta}_{g_i, \mathbb{H}_i}^\top(\tau_1), \dots, \boldsymbol{\theta}_{g_i, \mathbb{H}_i}^\top(\tau_K))^\top \in \mathbb{R}^{n_i K}$ and $\boldsymbol{\zeta}_{g_i} = (\boldsymbol{\zeta}_{g_i}^\top(\tau_1), \dots, \boldsymbol{\zeta}_{g_i}^\top(\tau_K))^\top \in \mathbb{R}^{K(p+1)}$, for $i \in [N]$. For convenience we rewrite the loss function of the node i as $\mathcal{L}_i(\boldsymbol{\theta}_{g_i, \mathbb{H}_i}, \boldsymbol{\zeta}_{g_i}) = (KT)^{-1} \sum_{k=1}^K \sum_{t=1}^T \rho_{\tau_k}(Y_{it} - \sum_j \theta_{g_i h_j}(\tau_k) w_{ij} Y_{j(t-1)} - \nu_{g_i}(\tau_k) Y_{i(t-1)} - \mathbf{x}_{it}^\top \boldsymbol{\gamma}_{g_i}(\tau_k))$ in this subsection. Specifically, denote $\widehat{\boldsymbol{\Phi}}_i = \{\widehat{\boldsymbol{\theta}}_{g, \mathbb{H}} : g \in [G], \mathbb{H} \in [H]^{n_i}\}$. As a result, $\widehat{\boldsymbol{\Phi}}_i$ collects possible estimated network interaction effects at K quantiles by exhausting all group memberships. Then we define the following profiled node-specific loss function as

$$\mathcal{L}_i^P(g) = \min_{\boldsymbol{\varphi}_i \in \widehat{\boldsymbol{\Phi}}_i} \mathcal{L}_i(\boldsymbol{\varphi}_i, \widehat{\boldsymbol{\zeta}}_g).$$

Define $\widehat{g}_i^\dagger = \arg \min_{g \in [G]} \mathcal{L}_i^P(g)$. If $\mathcal{L}_i^P(\widehat{g}_i^\dagger)$ is sufficiently smaller than $\mathcal{L}_i(\widehat{\boldsymbol{\theta}}_{\widehat{g}_i, \widehat{\mathbb{H}}_i}, \widehat{\boldsymbol{\zeta}}_{\widehat{g}_i})$, we then refine the membership estimate from \widehat{g}_i to \widehat{g}_i^\dagger . Specifically, the following refinement

protocol is used,

$$\widehat{g}_i^r = \begin{cases} \widehat{g}_i, & \text{if } \mathcal{L}_i(\widehat{\boldsymbol{\theta}}_{\widehat{g}_i, \widehat{\mathbb{H}}_i}, \widehat{\boldsymbol{\zeta}}_{\widehat{g}_i}) - \mathcal{L}_i^P(\widehat{g}_i^\dagger) \leq \frac{1}{\sqrt{T}} \mathcal{L}_i^P(\widehat{g}_i^\dagger) \\ \widehat{g}_i^\dagger, & \text{if } \mathcal{L}_i(\widehat{\boldsymbol{\theta}}_{\widehat{g}_i, \widehat{\mathbb{H}}_i}, \widehat{\boldsymbol{\zeta}}_{\widehat{g}_i}) - \mathcal{L}_i^P(\widehat{g}_i^\dagger) > \frac{1}{\sqrt{T}} \mathcal{L}_i^P(\widehat{g}_i^\dagger). \end{cases}$$

4.1.2 Refinement of \mathbb{H} Membership

Next, we refine the \mathbb{H} membership of the j th node. Recall that for the j th node, $\mathbb{F}_j = \{i : a_{ij} = 1\}$ is the set of its followers. The change of the membership h_j may affect the memberships in \mathbb{H}_i for $i \in \mathbb{F}_j$. Denote the collection of nodes in \mathcal{N}_i for $i \in \mathbb{F}_j$ as $\mathbb{F}_j^2 = \{l : \sum_i a_{il} a_{ij} \neq 0\}$, and additionally define $\widetilde{\mathbb{H}}_j = (h_l : l \in \mathbb{F}_j^2)^\top$. As a result, \mathbb{F}_j^2 collects the nodes who has a second order relationship with node j , whose column memberships can be affected by the change of h_j . Correspondingly, $\widetilde{\mathbb{H}}_j$ collects their column memberships and let $o_j = |\mathbb{F}_j^2|$. We define the following loss function for node j by fixing $h_j = h$ and exhausting possible memberships in $\widetilde{\mathbb{H}}_j$, i.e.,

$$\mathcal{H}_j^P(h) = \min_{\widetilde{\mathbb{H}}_j \in [H]^{o_j}, h_j = h} \sum_{i=1}^N a_{ij} \mathcal{L}_i(\widehat{\boldsymbol{\theta}}_{\widehat{g}_i^r, \widetilde{\mathbb{H}}_i}, \widehat{\boldsymbol{\zeta}}_{\widehat{g}_i^r}), \quad j = 1, \dots, N,$$

where $\widetilde{\mathbb{H}}_i \in \mathbb{R}^{n_i}$ is obtained by fixing $h_j = h$ and the other memberships are taken from $\widetilde{\mathbb{H}}_j$. In addition, the \mathbb{G} memberships are fixed as $g_i = \widehat{g}_i^r$ for all $i \in [N]$, and the estimated model parameters are also fixed.

Define $\widehat{h}_j^\dagger = \arg \min_{h \in [H]} \mathcal{H}_j^P(h)$. If $\mathcal{H}_j^P(\widehat{h}_j^\dagger)$ is sufficiently smaller than its unrefined counterpart $\sum_{i=1}^N a_{ij} \mathcal{L}_i(\widehat{\boldsymbol{\theta}}_{\widehat{g}_i^r, \widehat{\mathbb{H}}_i}, \widehat{\boldsymbol{\zeta}}_{\widehat{g}_i^r})$, we can refine the membership estimation \widehat{h}_j to \widehat{h}_j^\dagger .

Specifically, the following refinement protocol is used,

$$\widehat{h}_j^r = \begin{cases} \widehat{h}_j, & \text{if } \sum_{i=1}^N a_{ij} \mathcal{L}_i(\widehat{\boldsymbol{\theta}}_{\widehat{g}_i^r, \widehat{\mathbb{H}}_i}, \widehat{\boldsymbol{\zeta}}_{\widehat{g}_i^r}) - \mathcal{H}_j^P(\widehat{h}_j^\dagger) \leq \frac{1}{\sqrt{T}} \mathcal{H}_j^P(\widehat{h}_j^\dagger) \\ \widehat{h}_j^\dagger, & \text{if } \sum_{i=1}^N a_{ij} \mathcal{L}_i(\widehat{\boldsymbol{\theta}}_{\widehat{g}_i^r, \widehat{\mathbb{H}}_i}, \widehat{\boldsymbol{\zeta}}_{\widehat{g}_i^r}) - \mathcal{H}_j^P(\widehat{h}_j^\dagger) > \frac{1}{\sqrt{T}} \mathcal{H}_j^P(\widehat{h}_j^\dagger). \end{cases} \quad (4.1)$$

After obtaining the refined memberships $\widehat{\mathbb{G}}^r = (\widehat{g}_i^r : i \in [N])^\top$ and $\widehat{\mathbb{H}}^r = (\widehat{h}_j^r : j \in [N])$, one recompute the post-refined estimator $\widehat{\boldsymbol{\psi}}^r$ as $\widehat{\boldsymbol{\psi}}^r = \arg \min_{\boldsymbol{\psi}} \mathcal{L}(\boldsymbol{\psi}, \widehat{\mathbb{G}}^r, \widehat{\mathbb{H}}^r)$. In the following we first establish the estimation consistency for $\widehat{\mathbb{G}}^r$ and $\widehat{\mathbb{H}}^r$, which then leads to the asymptotic normality of $\widehat{\boldsymbol{\psi}}^r$.

4.2 Theoretical Analysis

4.2.1 Membership Estimation Consistency

In this section, we show that all group memberships can be consistently estimated after membership refinements. Let $\widehat{\mathcal{R}}_g^r = \{i : \widehat{g}_i^r = g\}$, $\mathcal{R}_{g_0}^0 = \{i : g_i^0 = g_0\}$, $\widehat{\mathcal{C}}_h^r = \{j : \widehat{h}_j^r = h\}$ and $\mathcal{C}_{h_0}^0 = \{j : h_j^0 = h_0\}$. The next theorem establish the membership estimation consistency for the \mathbb{G} groups.

Theorem 4. *Assume Conditions 1–6, if $G = G_0$ and $H = H_0$ hold. Then, we have*

(a) $\sup_{i \in [N]} K^{-1} \sum_{k=1}^K \|\widehat{\boldsymbol{\zeta}}_{\widehat{g}_i^r}(\tau_k) - \boldsymbol{\zeta}_{g_i^0}^0(\tau_k)\|^2 = o_p(1)$;

(b) *For any $g \in [G]$, there exists one $g_0 \in [G_0]$ such that $P(\widehat{\mathcal{R}}_g^r = \mathcal{R}_{g_0}^0) \rightarrow 1$.*

The proof of Theorem 4 is provided in Section A.6 in the supplementary material.

Subsequently, we proceed to establish the \mathbb{H} membership estimation consistency, which further requires the following assumption.

Assumption 7. *Assume that (a) $\sup_{j \in [N]} d_j^{-1} \min_{h \neq h_j^0} \{K^{-1} \sum_{k=1}^K \sum_{i=1}^N w_{ij}^2 |\theta_{g_i^0 h_j^0}^0(\tau_k) -$*

$\theta_{g_i^0 h}^0(\tau_k)|^2\} \geq c_0$ with $d_j = \sum_{i=1}^N a_{ij}$ being the in-degree of node j ; and that (b)

$$\max_{j \in [N]} \left(\sum_{i=1}^n w_{ij}^2 \right) \left(\frac{\bar{n} \log(NK)}{T} + N^{-1} |\mathcal{M}_H^c| \right) = o(1). \quad (4.2)$$

Assumption 7 (a) imposes a slightly more restrictive condition on interaction parameters concerning \mathbb{H} group differences than (3.1). Under the special case that $\max_j d_j < \infty$, Assumption 7 (a) is implied by (3.1), and hence can be removed. Assumption 7 (b) is related to the nodes' in-degrees, which puts restrictions on the diverging speed of $\max_j (\sum_{i=1}^n w_{ij}^2)$. If we have $\max_j d_j < \infty$, (4.2) can be automatically satisfied when $\bar{n} \log(NK)/T + N^{-1} |\mathcal{M}_H^c| = o(1)$. Under this condition, we can further prove the following Theorem.

Theorem 5. *Under Assumptions 1–7, if $G = G_0$ and $H = H_0$, then*

- (a) $\sup_{j \in [N]} \{(d_j K)^{-1} \sum_{i=1}^N \sum_{k=1}^K w_{ij}^2 |\hat{\theta}_{\hat{g}_i^r \hat{h}_j^r}(\tau_k) - \theta_{g_i^0 h_j^0}^0(\tau_k)|^2\} = o_p(1)$;
- (b) *For any $h \in [H]$, there exists one $h_0 \in [H_0]$ such that $P(\hat{\mathcal{C}}_h^r = \mathcal{C}_{h_0}^0) \rightarrow 1$.*

The proof of Theorem 5 is given in Section A.7 of the supplementary material. The consistency for \mathbb{H} memberships is relatively more difficult to show than for the \mathbb{G} memberships. Specifically, in conclusion (a), we first establish the uniform estimation consistency for $\hat{\theta}_{gh}(\tau_k)$ using the refined memberships \hat{h}_j^r . This enables us to further obtain the estimation consistency for \hat{h}_j^r as stated in conclusion (b). Lastly, with the result in Theorems 4 and 5, we can conclude that the post-refined estimator $\hat{\psi}^r$ is asymptotic equivalent to the oracle estimator as if the true memberships were known in advance. This enables us to conduct valid statistical inference using $\hat{\psi}^r$.

4.2.2 Asymptotic Normality

Note that when fixing $\mathbb{G} = \widehat{\mathbb{G}}^r$ and $\mathbb{H} = \widehat{\mathbb{H}}^r$, minimizing (2.5) is equivalent to minimizing $\mathcal{L}_{\tau_k}(\boldsymbol{\psi}, \widehat{\mathbb{G}}^r, \widehat{\mathbb{H}}^r)$ separately at each τ_k . Let $\boldsymbol{\xi}(\tau_k) = (\boldsymbol{\xi}_1(\tau_k)^\top, \dots, \boldsymbol{\xi}_{G_0}(\tau_k)^\top)^\top \in \mathbb{R}^{G_0(H_0+p+1)}$ with $\boldsymbol{\xi}_g(\tau_k)$ defined in (2.6), and write $\mathcal{X}_{it} = \mathbf{e}_{g_i^{(G_0)}} \otimes (\bar{\mathbf{y}}_i^\top, Y_{i(t-1)}, \mathbf{x}_{it}^\top)^\top \in \mathbb{R}^{G_0(H_0+p+1)}$ with $\bar{\mathbf{y}}_i = (\bar{Y}_h : h \in [H_0])^\top \in \mathbb{R}^{H_0}$ and $\bar{Y}_h = \sum_j I(h_j^0 = h) w_{ij} Y_{j(t-1)}$. Then we can express the model (2.1) as

$$\mathbf{y}_t = \mathbb{X}_t \boldsymbol{\xi}(\tau_k) + \boldsymbol{\varepsilon}_t(\tau_k),$$

where $\mathbb{X}_t = (\mathcal{X}_{it} : i \in [N]) \in \mathbb{R}^{N \times G_0(H_0+p+1)}$ and $\boldsymbol{\varepsilon}_t(\tau_k) = (\varepsilon_{it}(\tau_k) : i \in [N])^\top \in \mathbb{R}^N$. Denote the true parameter as $\boldsymbol{\xi}^0 = (\boldsymbol{\xi}^0(\tau_1)^\top, \dots, \boldsymbol{\xi}^0(\tau_K)^\top)^\top$, and define $\widehat{\boldsymbol{\xi}}^r(\tau_k)$ as the post-refined estimator when substituting $\mathbb{G} = \widehat{\mathbb{G}}^r$ and $\mathbb{H} = \widehat{\mathbb{H}}^r$. To establish the asymptotic normality of $\widehat{\boldsymbol{\xi}}^r(\tau_k)$, we further require the following conditions.

Assumption 8. *Assume that (a) $\boldsymbol{\Sigma}_f(\tau_k) = \lim_{N \rightarrow \infty} N^{-1} \sum_{i=1}^N \mathbb{E}\{f_{i\tau_k}(0|\mathcal{X}_{it}) \mathcal{X}_{it} \mathcal{X}_{it}^\top\}$ exists and nonsingular; (b) denote $\mathbf{g}_t(\tau_k) = N^{-1/2} \sum_{i=1}^N \{\tau_k - I(\varepsilon_{it}(\tau_k) < 0)\} \mathcal{X}_{it} \in \mathbb{R}^{G_0(H_0+p+1)}$ and assume $\boldsymbol{\Sigma}_{\mathcal{X}}(\tau_k) = \lim_{N, T \rightarrow \infty} \text{cov}(T^{-1/2} \sum_{t=1}^T \mathbf{g}_t(\tau_k))$ exists and is nonsingular. Let $\mathbb{E}(|\boldsymbol{\eta}^\top \mathbf{g}_t(\tau_k)|^\delta) < \infty$ for some constant $\delta > 2$ with any vector $\boldsymbol{\eta}$ satisfying $\|\boldsymbol{\eta}\| = 1$; and (c) $\gamma_1 \geq 1$ in Assumption 6.*

Assumption 8 (a) and (b) specify a set of moment conditions related to \mathbb{X}_t , where the matrices $\boldsymbol{\Sigma}_f(\tau_k)$ and $\boldsymbol{\Sigma}_{\mathcal{X}}(\tau_k)$ play important roles in the asymptotic covariance of $\widehat{\boldsymbol{\xi}}^r(\tau_k)$ as stated in Theorem 6. Next, Assumption 8 (c) prevents the tail for the distribution of Y_{it} from being too heavy. Compared to existing literature (Kato et al., 2012; Zhang et al., 2019), which typically assumes a bounded covariates assumption, condition (c) is more relaxed.

Theorem 6. *Assume that Assumptions 1–8 hold. Then we have that*

$$\sqrt{NT}(\widehat{\boldsymbol{\xi}}^r(\tau_k) - \boldsymbol{\xi}^0(\tau_k)) \rightarrow_d N(\mathbf{0}, \boldsymbol{\Sigma}_f(\tau_k)^{-1} \boldsymbol{\Sigma}_{\mathcal{X}}(\tau_k) \boldsymbol{\Sigma}_f(\tau_k)^{-1}).$$

The proof of Theorem 6 is provided in Section A.8 in the supplementary material. The proof follows the theoretical framework developed by [Kato et al. \(2012\)](#) for quantile panel data models, and the central limit theorems for dependent time series in [Fan and Yao \(2003\)](#). We remove the restriction that \mathcal{X}_{it} is uniformly bounded as required in [Kato et al. \(2012\)](#) to adapt for the applications in our scenario.

5 Simulation Studies

To examine the finite sample performance of the proposed method, we conducted a number of simulation studies with various network structures and parameter settings. Following [Koenker and Xiao \(2006\)](#) and [Zhu et al. \(2019b\)](#), we generate the data using the following data generating process

$$Y_{it} = \sum_{j=1}^N \theta_{g_i h_j}(U_{it}) w_{ij} Y_{j(t-1)} + \nu_{g_i}(U_{it}) Y_{i(t-1)} + \mathbf{x}_{it}^\top \boldsymbol{\gamma}_{g_i}(U_{it}), \quad (5.1)$$

where recall that $w_{ij} = a_{ij}/n_i$ denotes the element of the row-normalized weighting matrix. In this context, U_{it} 's are independently distributed variable following a uniform distribution between 0 and 1, which acts as noise in the data generation process. Additionally, $\theta_{g_i h_j}(\cdot)$, $\nu_{g_i}(\cdot)$ and $\boldsymbol{\gamma}_{g_i}(\cdot)$ are non-decreasing functions governing parameters of different groups. Assuming the right side of equation (5.1) is an increasing function

of U_{it} , the conditional quantile function $Q_{it}(\tau|\mathbf{x}_{it}, \mathcal{F}_{t-1})$ can be written as follows

$$Q_{it}(\tau|\mathbf{x}_{it}, \mathcal{F}_{t-1}) = \sum_{j=1}^N \theta_{g_i h_j}(\tau) w_{ij} Y_{j(t-1)} + \nu_{g_i}(\tau) Y_{i(t-1)} + \mathbf{x}_{it}^\top \boldsymbol{\gamma}_{g_i}(\tau),$$

which is consistent with (2.1).

Correspondingly, across all settings, the covariate vectors \mathbf{x}_{it} 's $\in \mathbb{R}^p$ are independently generated as absolute values of a multivariate normal distribution $N(\mathbf{0}, \mathbf{I}_p)$ with $p = 2$. For each network structure, we consider two settings with $G_0 = H_0 = 2$ and $G_0 = H_0 = 3$. When $G_0 = H_0 = 2$, the row membership ratios are determined by the parameters $(\pi_1^G, \pi_2^G) = (0.5, 0.5)$, and the column membership ratios are determined by $(\pi_1^H, \pi_2^H) = (0.4, 0.6)$. In the case of $G_0 = H_0 = 3$, we set the row and column membership ratios to be $(\pi_1^G, \pi_2^G, \pi_3^G) = (\pi_1^H, \pi_2^H, \pi_3^H) = (0.3, 0.3, 0.4)$. We considered two distinct network structures as follows.

1. **STOCHASTIC BLOCK MODEL (SBM).** In such networks, there are C communities composed of N nodes. If two nodes, denoted by i and j , belong to the same community, the probability they are connected is $P(a_{ij} = 1) = 6 \log(N)/N$; otherwise, the probability of connection is $P(a_{ij} = 1) = 2 \log(N)/N$. We conducted experiments with different network sizes of $N = 100, 200$, and set the number of communities to $C = 5, 10$, respectively.

2. **POWER-LAW DISTRIBUTION NETWORK.** In such a network, the in-degrees ($d_i = \sum_{j=1}^N a_{ji}$) of nodes is generated by a power-law distribution, which is common in real world networks such as social networks, where most nodes have only a limited number of followers while a few nodes have a large number of followers. According to [Clauset et al. \(2009\)](#), the network structure is constructed as follows. For each node i , we generate \tilde{d}_i by sampling from a power-law distribution where $P(\tilde{d}_i = k) \propto k^{-2.5}$

and then we set $d_i = 4\tilde{d}_i$. On this basis, for each node i , we randomly designate d_i nodes as its followers.

Under each network structure, we evaluate the performance of the proposed method under two different parameter settings.

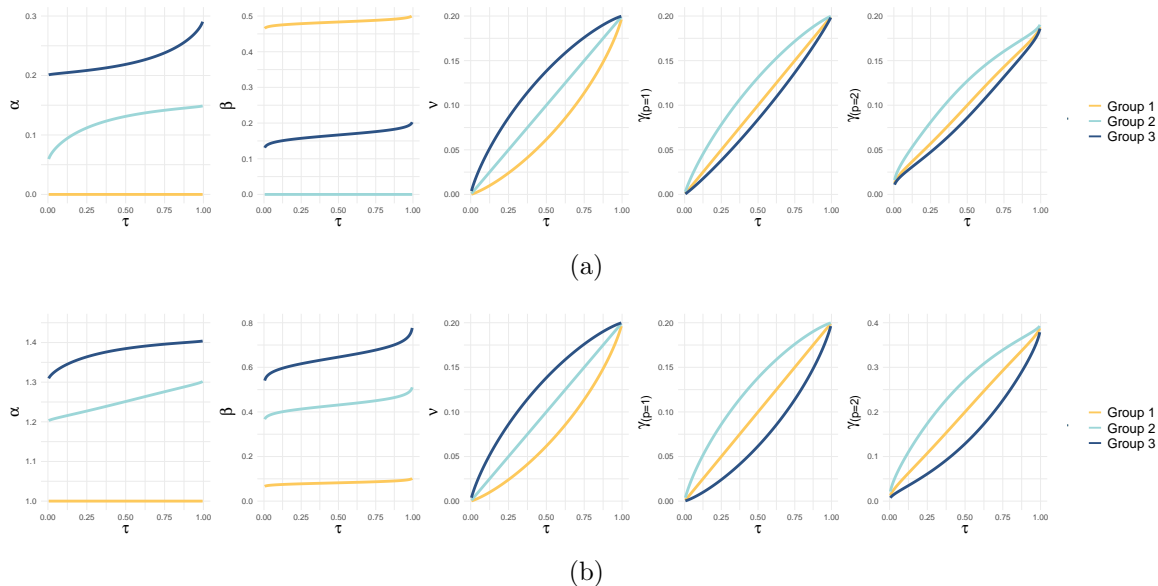


Figure 2: Relationships between parameters and τ . (a) Parameters for SCENARIO 1; (b) Parameters for SCENARIO 2.

In SCENARIO 1, we generate data using an additive model, specifying $\theta_{g_i h_j}(\tau)$ in an additive form as $\theta_{g_i h_j}(\tau) = \alpha_{g_i}(\tau) + \beta_{h_j}(\tau)$, while in SCENARIO 2, we generate data using a multiplicative model, where the network effects are considered as $\theta_{g_i h_j}(\tau) = \alpha_{g_i}(\tau) \times \beta_{h_j}(\tau)$. Figure 2 illustrates the shapes of these functions, the details of which are provided in Section A.2.2 of the supplementary material. The true parameters corresponding to the five quantiles $(\tau_1, \tau_2, \tau_3, \tau_4, \tau_5) = (0.1, 0.3, 0.5, 0.7, 0.9)$ for both scenarios are shown in Table 1.

Table 1: True parameters for SCENARIO 1 and SCENARIO 2.

SCENARIO	τ	α_1^0	α_2^0	α_3^0	ν_1^0	ν_2^0	ν_3^0	γ_{11}^0	γ_{21}^0	γ_{31}^0	γ_{12}^0	γ_{22}^0	γ_{32}^0	β_1^0	β_2^0	β_3^0
1	0.1	0.000	0.090	0.204	0.007	0.020	0.043	0.020	0.038	0.014	0.033	0.047	0.028	0.474	0.000	0.149
	0.3	0.000	0.117	0.210	0.031	0.060	0.098	0.060	0.090	0.047	0.065	0.091	0.054	0.480	0.000	0.159
	0.5	0.000	0.131	0.219	0.062	0.100	0.138	0.100	0.131	0.084	0.100	0.127	0.086	0.483	0.000	0.167
	0.7	0.000	0.140	0.233	0.102	0.140	0.169	0.140	0.164	0.125	0.135	0.155	0.122	0.487	0.000	0.174
	0.9	0.000	0.146	0.260	0.157	0.180	0.193	0.180	0.191	0.172	0.167	0.177	0.161	0.492	0.000	0.184
2	0.1	1.000	1.214	1.340	0.007	0.020	0.043	0.020	0.043	0.007	0.054	0.096	0.030	0.074	0.398	0.591
	0.3	1.000	1.232	1.369	0.031	0.060	0.098	0.060	0.098	0.031	0.126	0.196	0.073	0.079	0.417	0.623
	0.5	1.000	1.251	1.385	0.062	0.100	0.138	0.100	0.138	0.062	0.200	0.271	0.129	0.082	0.431	0.646
	0.7	1.000	1.271	1.394	0.102	0.140	0.169	0.140	0.169	0.102	0.274	0.327	0.204	0.086	0.446	0.670
	0.9	1.000	1.290	1.401	0.157	0.180	0.193	0.180	0.193	0.157	0.346	0.370	0.304	0.091	0.468	0.707

5.1 Estimation and Inference when $G = G_0$ and $H = H_0$

First, we evaluate the estimation performances when $G = G_0$ and $H = H_0$. Specifically, we apply general estimation procedure stated in Section 2.2 for both scenarios. Furthermore, we exploit the special model structures (i.e., additive model and multiplicative model) for estimation in SCENARIO 1 and SCENARIO 2 respectively with estimation procedures given in Section A.2.1 in the supplementary material, where the estimation results can be found in Section A.2.2 in the supplementary material to save space here. In both scenarios, we also evaluate the oracle estimators when the true memberships are given for comparison. We conduct model estimation separately at five quantile levels, i.e., $(\tau_1, \tau_2, \tau_3, \tau_4, \tau_5) = (0.1, 0.3, 0.5, 0.7, 0.9)$ for $B = 500$ repeated experiments. At each quantile level, the following metrics are calculated for measuring the estimation accuracy. For brevity, we omit the quantile index τ_k of the parameters in the subsequent sections. Let $\hat{\boldsymbol{\theta}}^{r(b)}$, $\hat{\boldsymbol{\nu}}^{r(b)}$ and $\hat{\boldsymbol{\gamma}}^{r(b)}$ be the refined estimators obtained from the b th simulation round. We calculate the root mean square error (RMSE) for $\boldsymbol{\theta}$ as $\text{RMSE}_{\boldsymbol{\theta}} = B^{-1} \sum_{b=1}^B \|\hat{\boldsymbol{\theta}}^{r(b)} - \boldsymbol{\theta}^0\|$. The RMSE for the other estimators can be similarly defined. Next, we conduct statistical inference for each estimator and construct 95% confidence intervals (CI) for each model parameter. Take

$\boldsymbol{\nu}^0$ for example, in the b th simulation round, we construct the 95% CI for ν_g^0 as $\text{CI}_{\boldsymbol{\nu},g}^{(b)} = (\widehat{\nu}_g^{r(b)} - 1.96\widehat{\text{SE}}_{\boldsymbol{\nu},g}^{(b)}, \widehat{\nu}_g^{r(b)} + 1.96\widehat{\text{SE}}_{\boldsymbol{\nu},g}^{(b)})$, where $\widehat{\text{SE}}_{\boldsymbol{\nu},g}^{(b)}$ is the estimated asymptotic standard error of $\widehat{\nu}_g^{r(b)}$ based on Theorem 6. For all components of $\boldsymbol{\nu}$, the average coverage error is computed as $\text{AE}_{\text{cp},\boldsymbol{\nu}} = G_0^{-1} \sum_{g=1}^{G_0} |B^{-1} \sum_{b=1}^B I(\nu_g^0 \in \text{CI}_{\boldsymbol{\nu},g}^{(b)}) - 0.95|$. Lastly, we calculate the row group membership estimation error as $\widehat{\varrho}_1^r = (NB)^{-1} \sum_{b=1}^B I(\widehat{g}_i^{r(b)} = g_i^0)$, where $\widehat{g}_i^{r(b)}$ corresponds to the refined row group membership estimator for node i from the b th simulation round (after label permutation). The column group membership estimation error rate denoted by $\widehat{\varrho}_2^r$ is defined similarly.

The simulation results for the SBM network are summarized in Tables 2 and 3. Simulations conducted on the power law networks yield similar results, details of which can be found in Section A.2.2 in the supplementary material. First, Tables 2 and 3 show that the accuracy of parameter estimation steadily improves as N or T increases at all quantile levels. Similarly, the group membership estimation error rates $\widehat{\varrho}_1^r$ and $\widehat{\varrho}_2^r$ significantly decrease as N and T grow. As expected, for fixed N and T , the proposed method performs much better under $G_0 = 2$ than under $G_0 = 3$, because the former has more data within each group to yield better estimation result. Furthermore, we observe lower AE_{cp} values for both scenarios when N and T are larger, which indicates a valid inference result. As N and T increase, the performance of the proposed estimation gradually approaches that of the oracle estimation. This lends further support to our theoretical findings in Theorem 6.

5.2 Estimation Performance with $G > G_0$ or $H > H_0$

In this section, we evaluate the performance of the proposed method under incorrectly specified group numbers, as well as the accuracy of group number estimation in Section 3.3. The true number of groups is fixed at $G_0 = 3$. To measure the

Table 2: RMSE's ($\times 10^{-2}$) and AE_{cp} 's (% , in the parenthesis) in SCENARIO 1 for the SBM network.

G	N	T	τ	Oracle estimator			TGNQ with refinement				
				$\hat{\theta}_o$	$\hat{\nu}_o$	$\hat{\gamma}_o$	$\hat{\theta}^r$	$\hat{\nu}^r$	$\hat{\gamma}^r$	$\hat{\varrho}_1^r(\%)$	$\hat{\varrho}_2^r(\%)$
2	100	50	0.1	5.0 (3.8)	1.8 (3.6)	0.9 (1.1)	6.1 (11.3)	1.9 (4.2)	1.0 (2.5)	2.8	6.8
			0.3	6.4 (1.7)	2.4 (2.0)	1.2 (1.2)	7.6 (8.4)	2.5 (2.6)	1.3 (3.4)		
			0.5	6.4 (1.2)	2.5 (1.6)	1.2 (1.4)	7.8 (8.7)	2.6 (2.0)	1.3 (2.7)		
			0.7	5.6 (2.6)	2.2 (1.0)	1.0 (1.0)	6.8 (9.7)	2.2 (1.0)	1.1 (2.6)		
			0.9	3.7 (3.2)	1.4 (1.3)	0.7 (1.1)	5.1 (12.8)	1.6 (2.2)	0.7 (2.5)		
	100	100	0.1	3.5 (3.2)	1.2 (1.4)	0.7 (0.7)	3.5 (4.2)	1.2 (1.6)	0.7 (1.0)	0.1	0.5
			0.3	4.5 (1.7)	1.7 (1.0)	0.8 (1.4)	4.5 (2.1)	1.7 (0.8)	0.8 (1.2)		
			0.5	4.5 (1.4)	1.7 (0.4)	0.8 (1.7)	4.6 (1.8)	1.7 (0.4)	0.8 (1.9)		
			0.7	3.9 (1.8)	1.5 (1.0)	0.7 (0.5)	4.0 (2.5)	1.5 (1.1)	0.7 (0.8)		
			0.9	2.6 (1.8)	1.0 (0.8)	0.5 (0.7)	2.6 (2.7)	1.0 (0.9)	0.5 (1.0)		
	100	200	0.1	2.5 (1.6)	0.9 (1.7)	0.5 (0.7)	2.5 (1.6)	0.9 (1.9)	0.5 (0.8)	0.0	0.0
			0.3	3.2 (0.8)	1.2 (0.9)	0.6 (0.7)	3.2 (0.9)	1.2 (1.0)	0.6 (0.7)		
			0.5	3.2 (1.2)	1.3 (1.4)	0.6 (0.5)	3.2 (1.2)	1.3 (1.4)	0.6 (0.5)		
			0.7	2.8 (1.9)	1.1 (0.2)	0.5 (0.8)	2.8 (1.9)	1.1 (0.3)	0.5 (0.9)		
			0.9	1.9 (2.2)	0.7 (0.1)	0.3 (0.3)	1.9 (2.3)	0.7 (0.1)	0.3 (0.3)		
	200	200	0.1	1.6 (1.4)	0.6 (1.2)	0.3 (0.7)	1.6 (1.5)	0.6 (1.3)	0.3 (0.8)	0.0	0.0
			0.3	2.1 (1.1)	0.9 (0.7)	0.4 (0.6)	2.1 (1.1)	0.9 (0.7)	0.4 (0.7)		
			0.5	2.1 (0.6)	0.9 (0.3)	0.4 (0.4)	2.1 (0.6)	0.9 (0.4)	0.4 (0.5)		
			0.7	1.7 (0.5)	0.7 (1.0)	0.3 (0.7)	1.8 (0.5)	0.7 (1.0)	0.3 (0.7)		
			0.9	1.2 (1.5)	0.6 (0.9)	0.2 (0.8)	1.2 (1.6)	0.6 (0.9)	0.2 (0.8)		
3	100	100	0.1	7.6 (2.8)	2.0 (2.7)	1.0 (1.4)	14.4 (24.4)	2.2 (5.1)	1.1 (4.8)	9.7	19.2
			0.3	10.2 (1.6)	2.7 (1.2)	1.3 (1.2)	17.9 (20.4)	3.0 (4.3)	1.5 (5.5)		
			0.5	10.7 (1.2)	3.0 (0.9)	1.4 (0.9)	19.2 (21.7)	3.3 (4.3)	1.7 (5.7)		
			0.7	9.7 (1.7)	2.6 (1.5)	1.3 (1.7)	16.9 (20.6)	2.9 (4.3)	1.4 (5.9)		
			0.9	7.0 (3.9)	1.9 (2.5)	0.9 (0.7)	13.7 (28.0)	2.1 (3.7)	1.0 (5.6)		
	100	200	0.1	5.4 (2.3)	1.4 (1.4)	0.7 (1.0)	7.0 (10.6)	1.4 (2.0)	0.7 (1.8)	3.0	7.6
			0.3	7.2 (1.2)	1.9 (1.1)	0.9 (1.4)	8.9 (7.5)	2.0 (1.7)	0.9 (1.8)		
			0.5	7.5 (1.0)	2.1 (0.9)	1.0 (1.3)	9.4 (7.1)	2.2 (1.3)	1.0 (1.6)		
			0.7	6.9 (1.6)	1.9 (0.9)	0.9 (0.8)	8.5 (8.3)	2.0 (1.9)	0.9 (1.6)		
			0.9	4.9 (2.4)	1.3 (0.5)	0.6 (1.1)	6.8 (14.5)	1.4 (1.5)	0.6 (1.6)		
	200	200	0.1	3.8 (2.2)	1.0 (1.0)	0.5 (0.9)	4.9 (9.7)	1.0 (1.7)	0.5 (2.5)	2.8	5.9
			0.3	4.8 (1.1)	1.4 (0.8)	0.7 (0.4)	5.8 (6.0)	1.4 (1.4)	0.7 (1.7)		
			0.5	5.0 (0.8)	1.5 (0.8)	0.7 (0.5)	5.9 (5.8)	1.5 (1.8)	0.7 (1.6)		
			0.7	4.4 (0.7)	1.3 (1.6)	0.6 (1.0)	5.3 (5.6)	1.4 (1.8)	0.6 (2.1)		
			0.9	3.2 (1.9)	1.0 (1.3)	0.4 (0.5)	4.3 (11.1)	1.0 (2.1)	0.4 (1.3)		
	200	400	0.10	2.7 (1.7)	0.7 (1.1)	0.4 (1.1)	2.8 (3.2)	0.7 (0.9)	0.4 (1.3)	0.3	1.4
			0.30	3.4 (1.0)	1.0 (0.7)	0.5 (0.6)	3.5 (1.7)	1.0 (0.9)	0.5 (0.6)		
			0.50	3.5 (0.5)	1.0 (0.7)	0.5 (0.6)	3.6 (1.0)	1.0 (0.7)	0.5 (0.4)		
			0.70	3.1 (0.7)	0.9 (0.8)	0.4 (0.8)	3.2 (1.2)	0.9 (1.1)	0.4 (0.5)		
			0.90	2.3 (0.9)	0.7 (0.3)	0.3 (1.2)	2.4 (3.6)	0.7 (0.9)	0.3 (1.3)		

Table 3: RMSE's ($\times 10^{-2}$) and AE_{cp} 's (% , in the parenthesis) in SCENARIO 2 for the SBM network.

G	N	T	τ	Oracle estimator			TGNQ with refinement				
				$\hat{\theta}_o$	$\hat{\nu}_o$	$\hat{\gamma}_o$	$\hat{\theta}^r$	$\hat{\nu}^r$	$\hat{\gamma}^r$	$\hat{\varrho}_1^r(\%)$	$\hat{\varrho}_2^r(\%)$
2	100	50	0.10	4.7 (2.3)	1.8 (2.5)	1.5 (1.4)	6.6 (15.7)	2.0 (5.7)	1.6 (3.3)	5.6	12.2
			0.30	6.1 (2.1)	2.4 (1.1)	1.9 (1.9)	8.7 (13.5)	2.5 (4.0)	2.1 (3.8)		
			0.50	6.1 (1.3)	2.5 (0.6)	1.9 (1.8)	9.0 (14.3)	2.7 (4.7)	2.1 (4.1)		
			0.70	5.5 (1.4)	2.3 (1.4)	1.7 (1.1)	7.7 (13.6)	2.4 (2.8)	1.8 (3.3)		
			0.90	3.9 (2.6)	1.6 (1.5)	1.1 (1.1)	6.5 (18.9)	1.8 (3.9)	1.2 (3.3)		
	100	100	0.10	3.3 (2.6)	1.3 (1.9)	1.1 (0.8)	3.6 (4.7)	1.3 (2.3)	1.1 (0.5)	0.5	2.1
			0.30	4.2 (1.6)	1.7 (1.1)	1.3 (1.4)	4.5 (3.2)	1.7 (0.6)	1.3 (1.5)		
			0.50	4.3 (1.4)	1.8 (1.0)	1.3 (1.3)	4.6 (2.3)	1.8 (0.8)	1.3 (1.4)		
			0.70	3.9 (2.2)	1.6 (1.1)	1.1 (1.0)	4.1 (3.5)	1.6 (1.0)	1.1 (1.0)		
			0.90	2.7 (1.6)	1.1 (1.2)	0.8 (0.8)	3.1 (4.4)	1.1 (1.2)	0.8 (1.6)		
	100	200	0.10	2.4 (1.7)	0.9 (1.9)	0.7 (0.9)	2.4 (1.7)	0.9 (1.7)	0.7 (0.9)	0.0	0.1
			0.30	3.1 (1.2)	1.2 (0.9)	0.9 (1.4)	3.1 (1.2)	1.2 (0.9)	0.9 (1.4)		
			0.50	3.1 (1.0)	1.3 (0.5)	0.9 (0.5)	3.1 (1.0)	1.3 (0.7)	0.9 (0.6)		
			0.70	2.8 (2.0)	1.2 (2.1)	0.8 (1.0)	2.8 (2.1)	1.2 (2.1)	0.8 (0.8)		
			0.90	2.0 (1.6)	0.8 (0.8)	0.6 (0.7)	2.0 (1.7)	0.8 (0.8)	0.6 (0.6)		
	200	200	0.10	1.6 (1.4)	0.6 (0.5)	0.5 (1.0)	1.6 (1.3)	0.6 (0.3)	0.5 (1.1)	0.0	0.1
			0.30	2.0 (1.4)	0.9 (1.4)	0.7 (0.7)	2.1 (1.5)	0.9 (1.3)	0.7 (0.7)		
			0.50	2.1 (0.7)	0.9 (0.2)	0.6 (0.5)	2.1 (0.7)	0.9 (0.2)	0.6 (0.4)		
			0.70	1.8 (0.6)	0.8 (0.4)	0.6 (1.0)	1.8 (0.7)	0.8 (0.3)	0.6 (1.1)		
			0.90	1.3 (1.1)	0.6 (0.5)	0.4 (0.8)	1.3 (1.5)	0.6 (0.6)	0.4 (0.9)		
3	100	100	0.10	7.9 (3.2)	2.0 (2.3)	1.5 (1.0)	13.5 (23.0)	2.1 (3.4)	1.6 (4.1)	7.4	14.1
			0.30	10.2 (1.4)	2.7 (1.7)	2.0 (1.4)	16.3 (18.0)	2.9 (3.5)	2.2 (4.0)		
			0.50	10.9 (1.2)	2.9 (0.7)	2.1 (0.7)	17.5 (18.0)	3.2 (3.1)	2.4 (4.1)		
			0.70	10.3 (1.7)	2.7 (1.6)	2.0 (1.5)	17.1 (19.0)	3.0 (3.8)	2.4 (4.9)		
			0.90	8.3 (2.9)	2.2 (3.1)	1.6 (0.8)	15.6 (25.4)	2.4 (3.4)	1.8 (4.7)		
	100	200	0.10	5.6 (2.4)	1.4 (1.1)	1.1 (1.1)	6.0 (4.6)	1.4 (1.2)	1.1 (1.4)	0.7	1.5
			0.30	7.3 (1.1)	1.9 (0.5)	1.4 (1.0)	7.7 (2.4)	1.9 (1.2)	1.4 (0.9)		
			0.50	7.8 (0.8)	2.1 (1.1)	1.5 (1.0)	8.1 (1.9)	2.1 (1.1)	1.5 (0.8)		
			0.70	7.4 (1.3)	2.0 (0.9)	1.4 (0.7)	7.8 (3.0)	2.0 (1.4)	1.5 (1.1)		
			0.90	5.9 (2.1)	1.5 (0.9)	1.1 (0.7)	6.5 (5.2)	1.6 (1.2)	1.1 (0.9)		
	200	200	0.10	4.0 (1.7)	1.0 (0.9)	0.8 (0.9)	4.3 (3.6)	1.0 (1.4)	0.8 (1.3)	0.9	1.3
			0.30	5.1 (1.0)	1.4 (0.7)	1.0 (0.5)	5.3 (2.1)	1.4 (0.6)	1.0 (1.0)		
			0.50	5.3 (0.8)	1.5 (0.6)	1.1 (0.6)	5.4 (1.6)	1.5 (0.5)	1.1 (0.9)		
			0.70	4.9 (0.6)	1.4 (1.3)	1.0 (1.1)	5.1 (1.2)	1.4 (1.5)	1.0 (1.0)		
			0.90	3.9 (1.0)	1.1 (1.5)	0.8 (0.9)	4.2 (3.3)	1.1 (1.4)	0.8 (1.3)		
	200	400	0.10	2.9 (1.4)	0.7 (0.9)	0.6 (1.1)	2.9 (1.4)	0.7 (0.8)	0.6 (0.9)	0.1	0.1
			0.30	3.6 (1.0)	1.0 (0.9)	0.7 (0.5)	3.6 (1.1)	1.0 (1.1)	0.7 (0.5)		
			0.50	3.7 (0.5)	1.0 (0.5)	0.7 (0.7)	3.7 (0.7)	1.0 (0.4)	0.7 (0.7)		
			0.70	3.5 (0.6)	1.0 (1.3)	0.7 (1.0)	3.5 (0.8)	1.0 (1.4)	0.7 (1.1)		
			0.90	2.8 (0.6)	0.8 (1.2)	0.5 (1.0)	2.8 (1.0)	0.8 (1.2)	0.5 (1.0)		

estimation accuracy under this setting, we use the following metrics. For the estimates of $\boldsymbol{\nu}^0$ and $\boldsymbol{\gamma}^0$, we define $\text{RMSE}_{\text{all},\boldsymbol{\nu}} = (NB)^{-1} \sum_{i=1}^N \sum_{b=1}^B |\widehat{\nu}_{g_i^{(b)}}^{(b)} - \nu_{g_i^0}^0|$ and $\text{RMSE}_{\text{all},\boldsymbol{\gamma}} = (NB)^{-1} \sum_{i=1}^N \sum_{b=1}^B \|\widehat{\boldsymbol{\gamma}}_{g_i^{(b)}}^{(b)} - \boldsymbol{\gamma}_{g_i^0}^0\|$. For the estimates of $\boldsymbol{\theta}^0$, we define $\text{RMSE}_{\text{all},\boldsymbol{\theta}} = N^{-2}B^{-1} \sum_{i=1}^N \sum_{j=1}^N \sum_{b=1}^B |\widehat{\theta}_{g_i^{(b)}h_j^{(b)}}^{(b)} - \theta_{g_i^0h_j^0}^0|$ to evaluate the estimation accuracy. We use $\widehat{\rho}_1$ and $\widehat{\rho}_2$ defined in (3.5) and (3.6) to measure the clustering error rates. In Table 4, for conciseness, we take the mean of these metrics corresponding to the five quantiles. In addition, we also use the QIC criterion proposed in (3.7) to select the group number, where we set the tuning parameter as $\lambda_{NT} = N^{1/10}T^{-1} \log(T)/(10 \min\{\bar{n}, 10\})$. We compute the model selection rate (MSR) as $\text{MSR}(G, H) = B^{-1} \sum_{b=1}^B I(\widehat{G}^{(b)} = G, \widehat{H}^{(b)} = H)$, for any given G and H , where $\widehat{G}^{(b)}$ and $\widehat{H}^{(b)}$ denotes the group number selected by QIC in the b th simulation run. In particular, $\text{MSR}(3,3)$ corresponds to the percentage of QIC correctly identifying the true number of groups $G_0 = 3$ and $H_0 = 3$.

From Table 4, we observe larger RMSEs when the model is under-fitted ($G = 2$ or $H = 2$), which suggests the significant model estimation bias caused by under-fitted models. When G and H are over-specified (i.e., $G > 3$ or $H > 3$), we observe that the RMSE and clustering errors are also slightly higher than the correctly specified model, which is possibly due to the overfitting effects under this case. Meanwhile, the MSR values $\text{MSR}(3,3)$ also gradually increase with larger N and T , which supports the results in Theorem 3. The MSR reaches 100% when N, T are large enough. In all cases, the resulting $\text{RMSE}_{\text{all},\cdot}$ is very close to that with fixed $G = G_0 = 3$ and $H = H_0 = 3$ when G and H are selected by QIC as \widehat{G} and \widehat{H} . Simulations on the power law networks produce comparable results, with additional details provided in Section A.2.2 of the supplementary material.

Table 4: Simulation results for the SBM network with varying G' s.

N	T	G	H	SCENARIO1						SCENARIO2					
				$\hat{\theta}$ (RMSE _{all} $\times 10^{-2}$)	$\hat{\nu}$	$\hat{\gamma}$	MSR (%)	$\hat{\varrho}_1$ (%)	$\hat{\varrho}_2$ (%)	$\hat{\theta}$ (RMSE _{all} $\times 10^{-2}$)	$\hat{\nu}$	$\hat{\gamma}$	MSR (%)	$\hat{\varrho}_1$ (%)	$\hat{\varrho}_2$ (%)
100	50	Oracle		0.8	0.4	0.2	-	-	-	0.8	0.4	0.3	-	-	-
		2	2	14.4	2.2	2.0	0.0	42.6	35.8	13.9	2.6	3.7	0.0	38.9	29.0
		2	3	18.5	2.4	2.0	1.6	44.0	37.4	12.1	2.5	3.3	8.2	34.8	20.0
		3	2	12.2	2.4	1.9	20.8	21.0	32.3	13.8	2.6	3.2	0.0	22.9	29.3
		3	3	15.9	2.5	1.9	70.2	22.5	34.5	11.8	2.6	3.1	78.6	20.6	20.7
		3	4	18.3	2.6	2.0	5.0	24.2	35.4	14.5	2.7	3.3	13.0	23.3	22.7
		4	3	17.3	3.4	2.5	2.4	24.1	35.8	13.6	3.3	3.9	0.2	23.2	22.8
		\hat{G}	\hat{H}	15.3	2.5	1.9	-	22.2	33.9	12.2	2.6	3.1	-	21.9	20.7
100	100	Oracle		2.4	1.2	0.6	-	-	-	2.4	1.2	1.0	-	-	-
		2	2	9.2	1.6	1.9	0.0	37.6	28.1	12.4	2.2	2.5	0.0	27.8	33.0
		2	3	10.6	1.6	1.9	0.0	38.5	25.0	11.0	2.1	2.4	0.2	26.6	20.7
		3	2	8.2	1.5	1.1	3.8	10.5	27.1	12.2	1.7	1.7	0.0	11.1	32.3
		3	3	8.0	1.5	1.1	94.8	10.1	20.5	7.8	1.6	1.5	92.4	7.5	14.2
		3	4	10.0	1.5	1.1	1.2	10.4	22.5	10.3	1.7	1.6	7.4	9.4	16.4
		4	3	9.8	2.1	1.5	0.2	12.8	23.4	9.8	2.0	2.2	0.0	10.8	17.7
		\hat{G}	\hat{H}	11.6	2.1	1.6	0.0	13.5	25.1	12.1	2.2	2.3	0.0	12.5	19.6
100	200	Oracle		1.7	0.9	0.4	-	-	-	1.7	0.9	0.7	-	-	-
		2	2	7.6	1.4	1.8	0.0	36.4	26.0	11.2	2.0	2.2	0.0	25.6	31.0
		2	3	5.7	1.3	1.8	0.0	36.2	8.9	8.3	2.0	2.1	0.0	24.5	13.8
		3	2	6.6	1.0	0.6	0.0	3.4	25.9	10.5	1.3	1.1	0.0	5.5	29.4
		3	3	3.6	0.9	0.6	100.0	3.0	7.6	2.3	0.9	0.7	100.0	0.7	1.6
		3	4	5.2	0.9	0.6	0.0	3.1	9.9	4.1	1.0	0.8	0.0	1.3	2.7
		4	3	4.5	1.3	0.9	0.0	4.7	8.8	3.2	1.3	1.2	0.0	1.4	2.4
		\hat{G}	\hat{H}	6.2	1.3	0.9	0.0	5.3	11.7	5.0	1.3	1.2	0.0	2.2	3.6
200	200	Oracle		1.1	0.6	0.3	-	-	-	1.2	0.6	0.5	-	-	-
		2	2	7.6	1.2	1.7	0.0	28.1	26.9	12.1	2.0	2.4	0.0	27.8	32.2
		2	3	4.8	1.2	1.7	0.0	28.0	6.1	7.4	2.0	2.2	0.0	26.5	11.2
		3	2	6.7	0.7	0.4	0.0	2.9	26.7	10.0	1.1	0.9	0.0	5.6	29.8
		3	3	2.6	0.7	0.4	100.0	2.8	5.9	1.7	0.7	0.5	100.0	0.9	1.3
		3	4	4.2	0.7	0.4	0.0	2.9	7.4	3.3	0.7	0.6	0.0	1.3	1.9
		4	3	3.3	1.0	0.8	0.0	2.9	6.4	2.3	1.0	1.1	0.0	1.0	1.4
		\hat{G}	\hat{H}	4.8	1.0	0.8	0.0	3.2	8.2	3.7	1.0	1.1	0.0	1.6	2.2
200	400	Oracle		0.8	0.4	0.2	-	-	-	0.8	0.4	0.3	-	-	-
		2	2	7.1	1.1	1.6	0.0	28.0	26.4	12.0	1.9	2.2	0.0	27.0	31.9
		2	3	3.9	1.1	1.6	0.0	28.0	1.6	6.5	1.9	2.1	0.0	26.1	8.7
		3	2	6.1	0.5	0.2	0.0	0.4	26.4	9.0	0.9	0.6	0.0	3.2	28.1
		3	3	1.1	0.4	0.2	100.0	0.3	1.4	0.9	0.4	0.3	100.0	0.1	0.1
		3	4	2.1	0.4	0.2	0.0	0.3	1.8	1.9	0.4	0.3	0.0	0.1	0.2
		4	3	1.5	0.6	0.5	0.0	0.3	1.5	1.2	0.7	0.7	0.0	0.1	0.1
		\hat{G}	\hat{H}	2.5	0.7	0.5	0.0	0.4	2.0	2.2	0.7	0.7	0.0	0.1	0.2
		\hat{G}	\hat{H}	1.1	0.4	0.2	-	0.3	1.4	0.9	0.4	0.3	-	0.1	0.1

5.3 Performance under Misspecified Models

In addition to the general estimation procedures outlined in Section 2.2, we propose model-specific estimation procedures for the Additive model and Multiplicative model in Appendix A.2.1 to more finely estimate the parameters. In this context, we proceed to investigate the robustness of the TGNQ model by studying its performance when the model is misspecified when $G = G_0$ and $H = H_0$. In SCENARIO 1, we employ the general, additive, and multiplicative models to estimate the parameters. Since the data is generated by the additive model, the multiplicative model represents a misspecified model in this case. In SCENARIO 2, we again utilize the general, additive, and multiplicative models to estimate the parameters, where the additive model is now a misspecified model. The summarized results are presented in Tables 5 and 6.

In Scenario 1, as shown in Table 5, we observe that when utilizing the mis-specified model to fit the data, the group membership estimation error rate rises slightly but remains acceptable. However, compared to the specified models, the root mean squared error (RMSE) of the fitted parameter θ^0 is higher and fails to decrease considerably with raising N and T . In Scenario 2, as shown in Table 6, we observe that there is almost no difference in the grouping error rates estimated by the three models. With the increase of N and T , they all achieve fairly good grouping accuracy. However, we find the parameters estimation by the mis-specified model still has a gap compared to the specified models, showing higher RMSE similarly. From the preceding analyses, the estimation methodology of the TGNQ model demonstrates appreciable robustness across varying scenarios. Results consistent with those obtained from simulations on power law networks are documented in Section A.2.2 of the supplementary material for further reference.

Table 5: RMSE's ($\times 10^{-2}$) in SCENARIO 1 for the SBM network and varying working models.

		$G=3$																																							
		General				Multiplicative(MIS)				Additive																															
N	T	τ	$\hat{\theta}$	$\hat{\nu}$	$\hat{\theta}_1$ (%)	$\hat{\theta}_2$ (%)	$\hat{\theta}$	$\hat{\nu}$	$\hat{\theta}_1$ (%)	$\hat{\theta}_2$ (%)	$\hat{\theta}$	$\hat{\nu}$	$\hat{\theta}_1$ (%)	$\hat{\theta}_2$ (%)	$\hat{\theta}$	$\hat{\nu}$	$\hat{\theta}_1$ (%)	$\hat{\theta}_2$ (%)																							
100	50	0.1	6.1	1.9	1.0	2.8	6.8	5.1	1.9	1.0	2.7	6.7	8.9	2.0	1.0	3.2	8.3	100	100	0.1	14.3	2.2	1.1	9.6	19.2	8.8	2.2	1.1	9.5	17.4	17.4	2.3	1.1	9.7	20.6						
		0.3	7.6	2.5	1.3	6.3	2.5	1.3	6.3	2.5	1.3	10.7	2.6	1.4	10.7	2.6	1.4	11.3	3.0	1.5	11.3	3.0	1.5	11.3	3.0	1.5	11.3	3.0	1.5	11.3	3.0	1.5	11.3	3.0	1.5	11.3	3.0	1.5			
		0.5	7.8	2.6	1.3	6.5	2.6	1.3	6.5	2.6	1.3	11.2	2.8	1.4	11.2	2.8	1.4	12.5	3.2	1.7	12.5	3.2	1.7	12.5	3.2	1.7	12.5	3.2	1.7	12.5	3.2	1.7	12.5	3.2	1.7	12.5	3.2	1.7			
		0.7	6.8	2.2	1.1	5.6	2.3	1.1	5.6	2.3	1.1	11.0	2.5	1.2	11.0	2.5	1.2	10.7	2.9	1.4	10.7	2.9	1.4	10.7	2.9	1.4	10.7	2.9	1.4	10.7	2.9	1.4	10.7	2.9	1.4	10.7	2.9	1.4	10.7	2.9	1.4
		0.9	5.1	1.6	0.7	4.0	1.6	0.7	4.0	1.6	0.7	10.9	1.8	0.9	10.9	1.8	0.9	8.6	2.0	1.0	8.6	2.0	1.0	8.6	2.0	1.0	8.6	2.0	1.0	8.6	2.0	1.0	8.6	2.0	1.0	8.6	2.0	1.0	8.6	2.0	1.0
100	100	0.1	3.5	1.2	0.7	0.1	0.5	2.9	1.2	0.7	0.1	0.5	7.0	1.6	0.7	0.2	0.8	100	200	0.1	7.0	1.4	0.7	2.9	7.5	4.6	1.4	0.7	2.9	7	14.9	1.7	0.8	3.1	12.7						
		0.3	4.5	1.7	0.8	3.7	1.7	0.8	3.7	1.7	0.8	8.8	2.1	0.9	8.8	2.1	0.9	5.9	2.0	0.9	5.9	2.0	0.9	5.9	2.0	0.9	5.9	2.0	0.9	5.9	2.0	0.9	5.9	2.0	0.9	5.9	2.0	0.9	5.9	2.0	0.9
		0.5	4.6	1.7	0.8	3.7	1.7	0.8	3.7	1.7	0.8	9.5	2.1	0.9	9.5	2.1	0.9	6.4	2.1	1.0	6.4	2.1	1.0	6.4	2.1	1.0	6.4	2.1	1.0	6.4	2.1	1.0	6.4	2.1	1.0	6.4	2.1	1.0	6.4	2.1	1.0
		0.7	4.0	1.5	0.7	3.2	1.5	0.7	3.2	1.5	0.7	9.8	1.9	0.8	9.8	1.9	0.8	5.7	2.0	0.9	5.7	2.0	0.9	5.7	2.0	0.9	5.7	2.0	0.9	5.7	2.0	0.9	5.7	2.0	0.9	5.7	2.0	0.9	5.7	2.0	0.9
		0.9	2.6	1.0	0.5	2.1	1.0	0.5	2.1	1.0	0.5	10.0	1.5	0.7	10.0	1.5	0.7	4.7	1.4	0.6	4.7	1.4	0.6	4.7	1.4	0.6	4.7	1.4	0.6	4.7	1.4	0.6	4.7	1.4	0.6	4.7	1.4	0.6	4.7	1.4	0.6
100	200	0.1	2.5	0.9	0.5	0.0	0.0	2.1	0.9	0.5	0.0	0.0	6.5	1.4	0.6	0.0	0.0	200	200	0.1	4.9	1.0	0.5	2.8	5.9	3.2	1.0	0.5	2.8	5.7	14.2	1.6	0.7	3.1	10.2						
		0.3	3.2	1.2	0.6	2.7	1.2	0.6	2.7	1.2	0.6	8.2	1.7	0.7	8.2	1.7	0.7	4.1	1.4	0.7	4.1	1.4	0.7	4.1	1.4	0.7	4.1	1.4	0.7	4.1	1.4	0.7	4.1	1.4	0.7	4.1	1.4	0.7	4.1	1.4	0.7
		0.5	3.2	1.3	0.6	2.6	1.3	0.6	2.6	1.3	0.6	9.0	1.8	0.7	9.0	1.8	0.7	4.4	1.5	0.7	4.4	1.5	0.7	4.4	1.5	0.7	4.4	1.5	0.7	4.4	1.5	0.7	4.4	1.5	0.7	4.4	1.5	0.7	4.4	1.5	0.7
		0.7	2.8	1.1	0.5	2.2	1.1	0.5	2.2	1.1	0.5	9.5	1.6	0.7	9.5	1.6	0.7	3.8	1.3	0.6	3.8	1.3	0.6	3.8	1.3	0.6	3.8	1.3	0.6	3.8	1.3	0.6	3.8	1.3	0.6	3.8	1.3	0.6	3.8	1.3	0.6
		0.9	1.9	0.7	0.3	1.4	0.7	0.3	1.4	0.7	0.3	9.8	1.4	0.6	9.8	1.4	0.6	3.1	1.0	0.4	3.1	1.0	0.4	3.1	1.0	0.4	3.1	1.0	0.4	3.1	1.0	0.4	3.1	1.0	0.4	3.1	1.0	0.4	3.1	1.0	0.4
200	200	0.1	1.6	0.6	0.3	0.0	0.0	1.3	0.6	0.3	0.0	0.0	6.3	1.5	0.5	0.0	0.1	200	400	0.1	2.8	0.7	0.4	0.3	1.4	1.9	0.7	0.4	0.3	1.3	13.8	1.5	0.6	0.4	5.8						
		0.3	2.1	0.9	0.4	1.7	0.8	0.4	1.7	0.8	0.4	7.7	1.7	0.6	7.7	1.7	0.6	2.4	1.0	0.5	2.4	1.0	0.5	2.4	1.0	0.5	2.4	1.0	0.5	2.4	1.0	0.5	2.4	1.0	0.5	2.4	1.0	0.5	2.4	1.0	0.5
		0.5	2.1	0.9	0.4	1.8	0.9	0.4	1.8	0.9	0.4	8.3	1.7	0.7	8.3	1.7	0.7	2.6	1.0	0.5	2.6	1.0	0.5	2.6	1.0	0.5	2.6	1.0	0.5	2.6	1.0	0.5	2.6	1.0	0.5	2.6	1.0	0.5	2.6	1.0	0.5
		0.7	1.8	0.7	0.3	1.5	0.7	0.3	1.5	0.7	0.3	8.7	1.6	0.7	8.7	1.6	0.7	2.3	0.9	0.4	2.3	0.9	0.4	2.3	0.9	0.4	2.3	0.9	0.4	2.3	0.9	0.4	2.3	0.9	0.4	2.3	0.9	0.4	2.3	0.9	0.4
		0.9	1.2	0.6	0.2	1.0	0.5	0.2	1.0	0.5	0.2	9.1	1.6	0.7	9.1	1.6	0.7	1.7	0.7	0.3	1.7	0.7	0.3	1.7	0.7	0.3	1.7	0.7	0.3	1.7	0.7	0.3	1.7	0.7	0.3	1.7	0.7	0.3	1.7	0.7	0.3

Table 6: RMSE's ($\times 10^{-2}$) in SCENARIO 2 for the SBM network and varying working models.

		$G=3$																																							
		General				Multiplicative				Additive(MIS)																															
N	T	τ	$\hat{\theta}$	$\hat{\nu}$	$\hat{\theta}_1$ (%)	$\hat{\theta}_2$ (%)	$\hat{\theta}$	$\hat{\nu}$	$\hat{\theta}_1$ (%)	$\hat{\theta}_2$ (%)	$\hat{\theta}$	$\hat{\nu}$	$\hat{\theta}_1$ (%)	$\hat{\theta}_2$ (%)	$\hat{\theta}$	$\hat{\nu}$	$\hat{\theta}_1$ (%)	$\hat{\theta}_2$ (%)																							
100	50	0.1	6.6	2.0	1.6	5.6	12.2	5.5	2.0	1.6	5.5	12.2	6.6	2.0	1.7	5.6	12.5	100	100	0.1	13.5	2.1	1.6	7.4	14.1	9.1	2.1	1.6	6.6	12.3	13.5	2.2	1.6	7.6	14.1						
		0.3	8.7	2.5	2.1	7.4	2.5	2.1	7.4	2.5	2.1	8.4	2.5	2.1	8.4	2.5	2.1	10.7	2.8	2.2	10.7	2.8	2.2	10.7	2.8	2.2	10.7	2.8	2.2	10.7	2.8	2.2	10.7	2.8	2.2	10.7	2.8	2.2			
		0.5	9.0	2.7	2.1	7.9	2.7	2.1	7.9	2.7	2.1	9.3	2.7	2.1	9.3	2.7	2.1	11.5	3.1	2.4	11.5	3.1	2.4	11.5	3.1	2.4	11.5	3.1	2.4	11.5	3.1	2.4	11.5	3.1	2.4	11.5	3.1	2.4	11.5	3.1	2.4
		0.7	7.7	2.4	1.8	6.7	2.4	1.8	6.7	2.4	1.8	8.6	2.4	1.8	8.6	2.4	1.8	11.3	3.0	2.3	11.3	3.0	2.3	11.3	3.0	2.3	11.3	3.0	2.3	11.3	3.0	2.3	11.3	3.0	2.3	11.3	3.0	2.3	11.3	3.0	2.3
		0.9	6.5	1.8	1.2	5.5	1.8	1.2	5.5	1.8	1.2	8.1	1.8	1.2	8.1	1.8	1.2	10.7	2.3	1.8	10.7	2.3	1.8	10.7	2.3	1.8	10.7	2.3	1.8	10.7	2.3	1.8	10.7	2.3	1.8	10.7	2.3	1.8	10.7	2.3	1.8
100	100	0.1	3.6	1.3	1.1	0.5	2.1	1.3	1.1	0.5	2	4.7	1.3	1.1	4.7	1.3	1.1	4.3	1.4	1.1	4.3	1.4	1.1	4.3	1.4	1.1	4.3	1.4	1.1	4.3	1.4	1.1	4.3	1.4	1.1	4.3	1.4	1.1	4.3	1.4	1.1
		0.3	4.5	1.7	1.3	3.8	1.7	1.3	3.8	1.7	1.3	5.6	1.7	1.3	5.6	1.7	1.3	6.0	1.8	1.3	6.0	1.8	1.3	6.0	1.8	1.3	6.0	1.8	1.3	6.0	1.8	1.3	6.0	1.8	1.3	6.0	1.8	1.3	6.0	1.8	1.3
		0.5	4.6	1.8	1.3	3.7	1.8	1.3	3.7	1.8	1.3	6.0	1.8	1.3	6.0	1.8	1.3	6.2	1.6	1.1	6.2	1.6	1.1	6.2	1.6	1.1	6.2	1.6	1.1	6.2	1.6	1.1	6.2	1.6	1.1	6.2	1.6	1.1	6.2	1.6	1.1
		0.7	4.1	1.6	1.1	3.3	1.6	1.1	3.3	1.6	1.1	6.2	1.6	1.1	6.2	1.6	1.1	5.7	2.0	1.4	5.7	2.0	1.4	5.7	2.0	1.4	5.7	2.0	1.4	5.7	2.0	1.4	5.7	2.0	1.4	5.7	2.0	1.4	5.7	2.0	1.4
		0.9	3.1	1.1	0.8	2.5	1.1	0.8	2.5	1.1	0.8	6.3	1.2	0.8	6.3	1.2	0.8	4.7	1.5	1.1	4.7	1.5	1.1	4.7	1.5	1.1	4.7	1.5	1.1	4.7	1.5	1.1	4.7	1.5	1.1	4.7	1.5	1.1	4.7	1.5	1.1
100	200	0.1	2.4	0.9	0.7	0.0	0.1	2.0	0.9	0.7	0.0	0.1	4.1	0.9	0.7	0.0	0.3	200	200	0.1	4.3	1.0	0.8	0.9	1.3	3.1	1.0	0.8	0.9	1.2	10.3	1.5	0.8	1.2	3						

6 Real Data Example

6.1 Data Description

In this section, we illustrate the proposed methodology with a stock dataset, which consists of quarterly data on 651 A-share stocks listed on Chinese stock exchanges from the third quarter of 2011 to the second quarter of 2023. We construct a financial network among firms based on their common top ten investors in each period. This approach is in line with prior researches, exemplified by studies such as [Zhu et al. \(2019b\)](#) and [Chen et al. \(2023\)](#). Constructing networks among firms with shared ownership helps us to quantify the spillover effects among the stocks, as highlighted by previous literature. For instance, [Anton and Polk \(2014\)](#) investigate variations in return covariance due to common active mutual fund ownership. [Li et al. \(2016\)](#) explore market volatility prediction using network diameter based on common shareholders of listed companies.

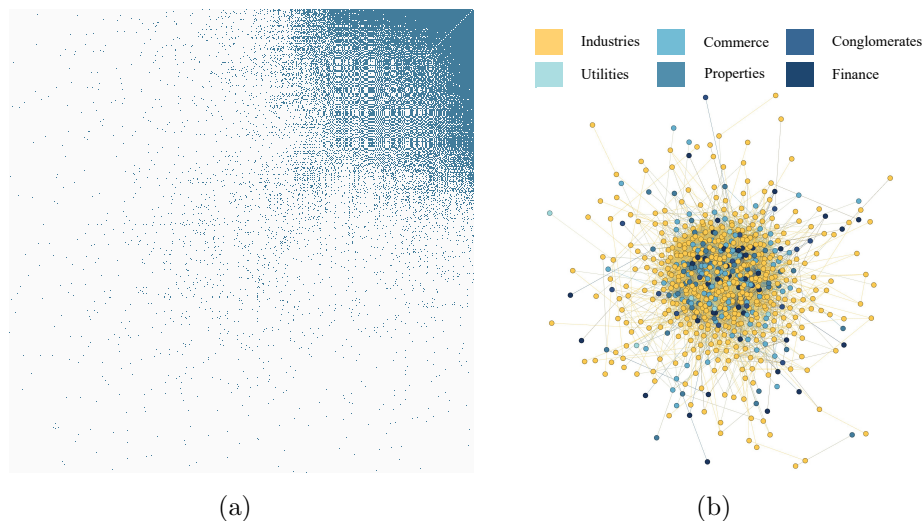


Figure 3: (a) The heatmap of the adjacency matrix among the stocks; (b) The visualization of stock network.

Specifically, the adjacency matrix \mathbf{A} captures intertwined ownership structures, wherein $a_{ij} = 1$ denotes that firms i and j possess three or more significant shareholders

in common for all quarters, while 0 signifies the absence of such shared ownership. The adjacency matrix \mathbf{A} and corresponding network relationships are illustrated in Figure 3, where we observe a small portion of companies share denser network links, with the majority of them belonging to the same industrial sector.

We then define a dependent variable as the log quarterly volatility, defined by

$$Y_{it} = \log \left[(D_t - 1)^{-1} \sum_{d=2}^{D_t} (\log P_{it,d} - \log P_{it,d-1})^2 \right]$$

where $P_{it,d}$ denotes the closing price of stock i on day d of quarter t and D_t denotes the number of trading days in quarter t . Previously, a similar measurement approach has been employed in the literature (Huang et al., 2021) to investigate the network connections among publicly traded stocks. This constitutes a panel data with $N = 651$ firms over $T = 47$ quarters.

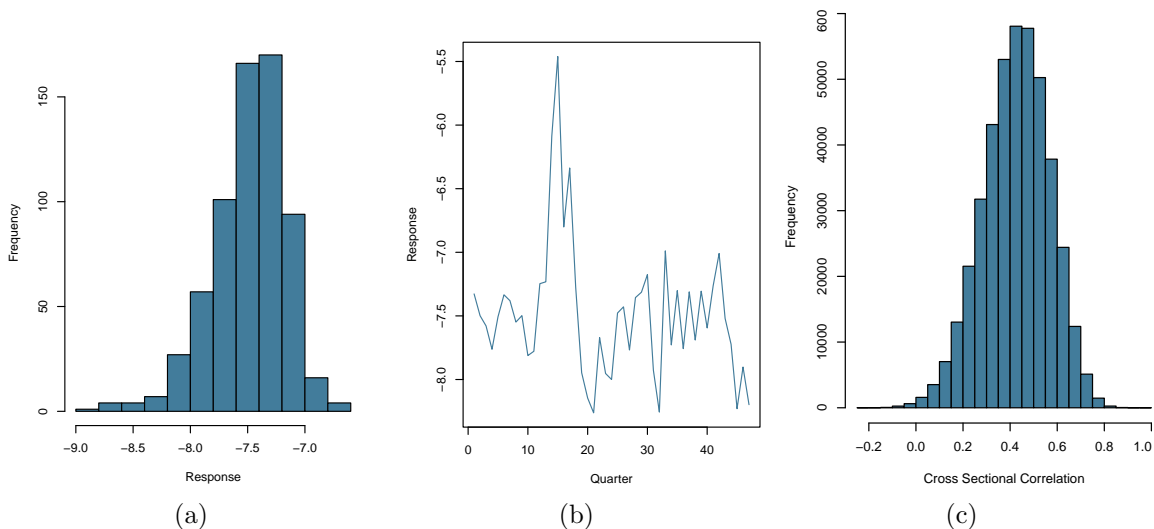


Figure 4: (a) Histogram of firm-level averages of the responses; (b) Time series of cross-sectional averages of the responses over different companies; (c) Histogram of pairwise cross-sectional correlations.

Figure 4(a) shows the distribution of the mean response computed at the firm level, where the median rests at -7.45. Moreover, Figure 4(b) presents the time series

trajectory of the cross-sectional average response over the all firms, spanning 47 quarters. Notably, the average response through 14th to the 17th quarter exhibits higher volatility values. Additionally, Figure 4(c) constitutes a histogram of the $N(N - 1)/2$ pairwise correlations of response for all combinations of the 651 firms, i.e. the sample correlation of $\{Y_{it} : 1 \leq t \leq T\}$ and $\{Y_{jt} : 1 \leq t \leq T\}$ for all $i \neq j$. The mean sample correlation stands at 0.425, conveying moderate positive comovement in volatility on average.

Finally, we include six covariates, which are collected from the companies' quarterly financial disclosures. They are, respectively, SIZE (log-transformed market value), BM (book to market ratio), PR (increased profit ratio compared to the last year), AR (increased asset ratio compared to the last year), LEV (log-transformed leverage ratio), and CF (cash flow). These metrics are inspired by the research of [Fama and French \(2015\)](#) and have also been used in other studies for financial risk factor analysis ([Fan et al., 2022](#)). Our modelling approach and results are detailed in the following section.

6.2 Model Estimation Results

In order to apply the TGNQ model to the aforementioned dataset, the foremost task is to select the numbers of groups, i.e., G and H . We take $\lambda_{NT} = N^{1/10}T^{-1} \log(T) / (10 \min\{\bar{n}, 10\})$, as done in the simulation study (recall that \bar{n} is the average out-degree of the nodes). Suggested by the QIC values as shown in Figure 5, we obtain estimates that $\hat{G} = 2$ and $\hat{H} = 3$.

The model estimation results are visualized in Figures 6 at quantiles $\tau = 0.1, 0.3, 0.5, 0.7$ and 0.9 . More detailed parameter estimates can be found in Appendix A.2.3. First, we observe that at almost all quantiles, the autoregressive effect and network effect are

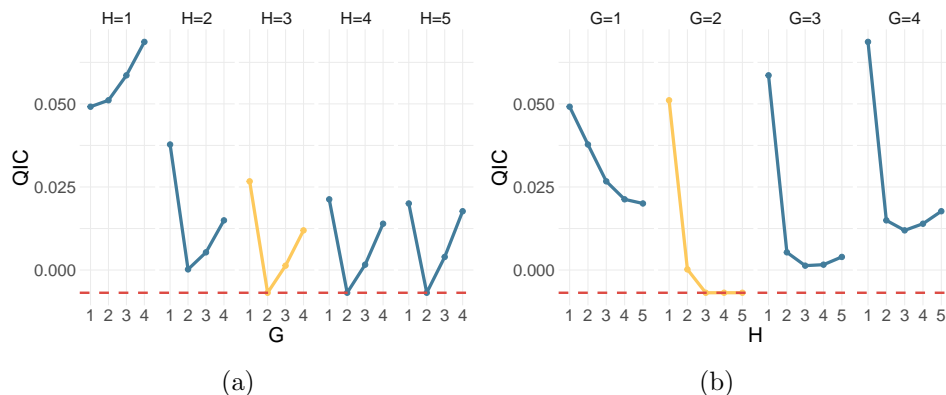


Figure 5: QIC values for $1 \leq G \leq 4$ and $1 \leq H \leq 5$.

significantly positive across all groups. This indicates that stock volatility is influenced not only by its own historical performance but also by the volatility of connected stocks. In addition, at the upper tail (i.e. $\tau = 0.9$), the estimated autoregressive effect is smaller while the network effect is larger. This means when the market is exposed to higher levels of volatility, stocks tend to have higher correlations through the network. This is consistent with the conclusion drawn from related studies, which found a significant increase in the correlation of stocks during periods of abnormal volatility in global or major regional stock market (Kaminsky et al., 2001; Gross and Kok, 2013). In contrast, under lower levels of volatility, the estimated autoregressive effect is larger while the network effect is smaller, indicating stocks are mainly influenced by their own historical performance.

Furthermore, at the upper tail (i.e., $\tau = 0.9$), the second row group exhibits a larger autoregressive effect and a smaller network effect compared to the first row group. This indicates that when the market faces higher levels of volatility, the first row group is more susceptible to volatility spreading through network connections compared to the second row group. At the lower tail (i.e., $\tau = 0.1$), the autoregressive effects of the two row groups are very close. Under normal volatility levels (i.e., $\tau = 0.5$), both groups have small network effects. Additionally, at the upper tail, the first column group has

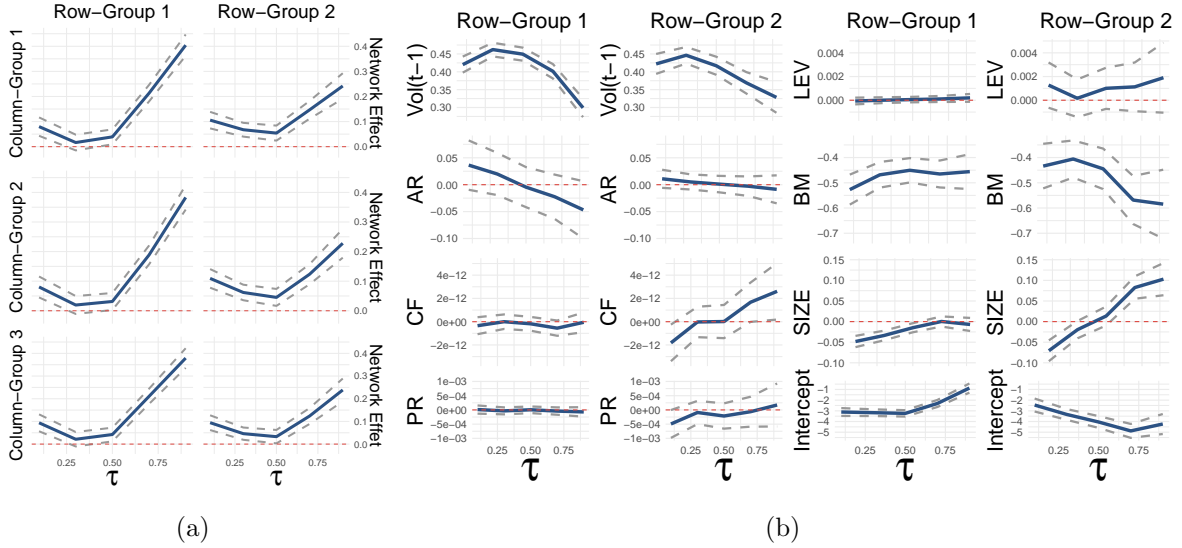


Figure 6: (a) Quantile regression parameter estimators of network effects with 95% confidence interval bounds; (b) Quantile regression parameter estimators of autoregressive and covariate effects with 95% confidence interval bounds.

a larger network effect than the other two column groups, indicating that it can exert more influence on connected stocks under high market volatility.

Subsequently, we comment on the estimation results of the covariates. First, at all quantiles, the volatility levels of all groups are negatively correlated with the BM value. This is highly correlated with the finding of [Fama and French \(1992\)](#) that the BM value represents a risk factor, with the conclusion that stocks with lower BM values have higher risk. Furthermore, at low to moderate levels of volatility ($\tau = 0.1, 0.3, 0.5$), the SIZE value is significantly negatively correlated with the volatility of the first row group, but this relationship becomes insignificant at high quantile levels ($\tau = 0.7, 0.9$). In contrast, the relationship between SIZE and the volatility of the second row group is negative at the lower tail and positive at the upper tail. Moreover, only the volatility of the second row group is negatively correlated with the relative increase in PR at the lower tail ($\tau = 0.1$). Additionally, the volatility of the second group is significantly correlated with the CF value, exhibiting a significant negative effect at $\tau = 0.1$ and a

significant positive effect at $\tau = 0.9$. This indicates that while larger cash flows further stabilize the volatility levels of stocks in the second group during relatively calm market conditions, they exacerbate the volatility of stocks in the second group during periods of high market volatility.

Finally, we present several descriptive analysis for better understanding the clustering results. Firstly, Figure 7(a) shows the distribution of cross-sectional mean responses within each group. It can be observed that the median of the second row group is higher than that of the first row group, while the median of the second column group is higher than the other two column groups. To better understand the differences between these groups, Figure 7(b) visualizes the average covariate values across different groups. The LEV, AR and CF values of the first row group are markedly lower than those of the second row group. The difference in PR values between these two groups is even larger, with the first row group having a positive average PR value and the second group a negative one. For the three column groups, the first column group has a negative average PR value which differs notably from the other groups, and its LEV value is also markedly lower than the other two groups, but its AR value is the highest. The second column group has the lowest AR value among all column groups, yet the highest CF value. The third column group has a PR value much higher than the other column groups, but a CF value markedly lower than the other column groups.

7 Conclusion

This paper propose a two-way grouped network quantile panel data model to characterize both cross-sectional and temporal dependence in a network context. The model incorporates a novel two-way group structure that allows each unit to have distinct “re-

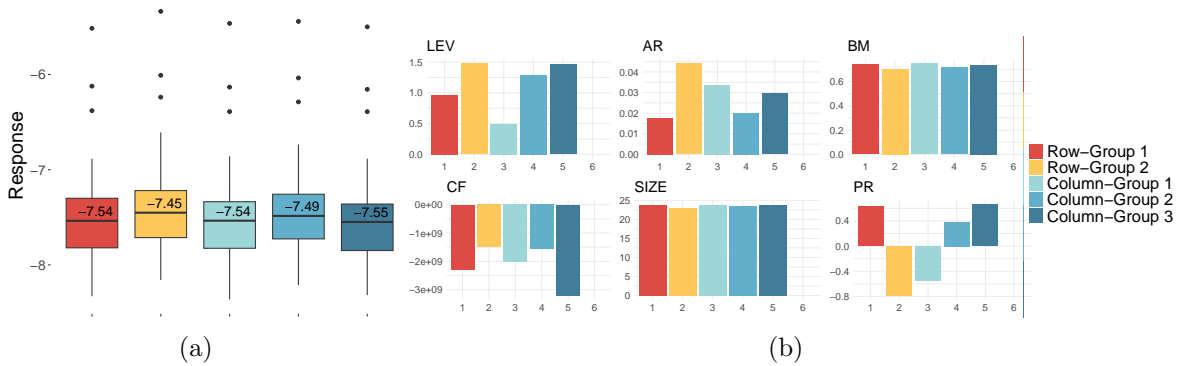


Figure 7: (a) Distributions of cross-sectional mean responses within each group; (b) Average covariate values across groups.

ceiving” and “influencing” group memberships, thereby capturing potential directional influences among different groups in the network. We develop an efficient algorithm to estimate the TGNQ model parameters and establish important asymptotic properties, including consistency of the estimators when the group numbers are overspecified and asymptotic normality when the true group numbers are known. Additionally, we propose a data-driven criterion to consistently select the true group numbers. Moreover, extensive simulations demonstrate a desirable finite sample performance of the estimation method across varying data generating processes and network structures, accurately recovering latent groups and network effects. Furthermore, robustness to model misspecification is also illustrated. Finally, an empirical application to volatility modelling of Chinese stocks highlight the usefulness of the framework in uncovering insightful group patterns and quantifying complex network.

To conclude the article, we explore various compelling directions for future research. Extensions to accommodate time-varying network structures would enable the modelling of dynamic network evolutions, offering deeper insights into evolving interconnections among units over time. Furthermore, exploring flexible semi/non-parametric specifications could enhance the ability of model to capture complex nonlinear covariate effects, thus widening its applicability to a broader range of empirical contexts.

Finally, theoretical investigations into the consistency of estimation under scenarios involving a growing number of covariates would constitute a valuable contribution, offering a more comprehensive understanding of the model's properties and enhancing its practical utility in empirical research.

References

- Abbe, E., Fan, J., and Wang, K. (2022), “An ℓ_p theory of PCA and spectral clustering,” *The Annals of Statistics*, 50, 2359–2385.
- Abbe, E., Fan, J., Wang, K., and Zhong, Y. (2020), “Entrywise eigenvector analysis of random matrices with low expected rank,” *Annals of Statistics*, 48, 1452.
- Abrevaya, J. and Dahl, C. M. (2008), “The effects of birth inputs on birthweight: evidence from quantile estimation on panel data,” *Journal of Business & Economic Statistics*, 26, 379–397.
- Ando, T. and Bai, J. (2016), “Panel data models with grouped factor structure under unknown group membership,” *Journal of Applied Econometrics*, 31, 163–191.
- (2017), “Clustering huge number of financial time series: A panel data approach with high-dimensional predictors and factor structures,” *Journal of the American Statistical Association*, 112, 1182–1198.
- Ando, T., Li, K., and Lu, L. (2023), “A spatial panel quantile model with unobserved heterogeneity,” *Journal of Econometrics*, 232, 191–213.
- Anton, M. and Polk, C. (2014), “Connected stocks,” *The Journal of Finance*, 69, 1099–1127.

- Benham, T., Duan, Q., Kroese, D., and Liquet, B. (2017), “CEoptim: Cross-entropy R package for optimization,” *Journal of Statistical Software*, 76, 1–29.
- Bester, C. A. and Hansen, C. B. (2016), “Grouped effects estimators in fixed effects models,” *Journal of Econometrics*, 190, 197–208.
- Bonhomme, S. and Manresa, E. (2015), “Grouped patterns of heterogeneity in panel data,” *Econometrica*, 83, 1147–1184.
- Bougerol, P. and Picard, N. (1992), “Strict stationarity of generalized autoregressive processes,” *The Annals of Probability*, 20, 1714–1730.
- Chen, E. Y., Fan, J., and Zhu, X. (2023), “Community network auto-regression for high-dimensional time series,” *Journal of Econometrics*, 235, 1239–1256.
- Chen, L., Dolado, J. J., and Gonzalo, J. (2021), “Quantile factor models,” *Econometrica*, 89, 875–910.
- Chen, X. and Tokdar, S. T. (2021), “Joint quantile regression for spatial data,” *Journal of the Royal Statistical Society Series B: Statistical Methodology*, 83, 826–852.
- Choi, D. and Wolfe, P. J. (2014), “Co-clustering separately exchangeable network data,” *The Annals of Statistics*, 42, 29–63.
- Clauset, A., Shalizi, C. R., and Newman, M. E. (2009), “Power-law distributions in empirical data,” *SIAM Review*, 51, 661–703.
- Diebold, F. X. and Yilmaz, K. (2014), “On the network topology of variance decompositions: Measuring the connectedness of financial firms,” *Journal of Econometrics*, 182, 119–134.

- Dou, B., Parrella, M. L., and Yao, Q. (2016), “Generalized Yule–Walker estimation for spatio-temporal models with unknown diagonal coefficients,” *Journal of Econometrics*, 194, 369–382.
- Fama, E. F. and French, K. R. (1992), “The cross-section of expected stock returns,” *the Journal of Finance*, 47, 427–465.
- (2015), “A five-factor asset pricing model,” *Journal of Financial Economics*, 116, 1–22.
- Fan, J., Guo, J., and Zheng, S. (2022), “Estimating number of factors by adjusted eigenvalues thresholding,” *Journal of the American Statistical Association*, 117, 852–861.
- Fan, J. and Yao, Q. (2003), *Nonlinear Time Series: Nonparametric and Parametric Methods*, vol. 20, Springer.
- Fang, G., Xu, G., Xu, H., Zhu, X., and Guan, Y. (2023), “Group network Hawkes process,” *Journal of the American Statistical Association*, 1–17.
- Foss, S., Korshunov, D., Zachary, S., et al. (2011), *An Introduction to Heavy-tailed and Subexponential Distributions*, vol. 6, Springer.
- Galvao, A. F. and Kato, K. (2016), “Smoothed quantile regression for panel data,” *Journal of Econometrics*, 193, 92–112.
- Gross, M. and Kok, C. (2013), “Measuring contagion potential among sovereigns and banks using a mixed-cross-section GVAR,” Tech. rep., ECB Working Paper.
- Gu, J. and Volgushev, S. (2019), “Panel data quantile regression with grouped fixed effects,” *Journal of Econometrics*, 213, 68–91.

- Härdle, W. K., Wang, W., and Yu, L. (2016), “Tenet: Tail-event driven network risk,” *Journal of Econometrics*, 192, 499–513.
- He, X., Pan, X., Tan, K. M., and Zhou, W. X. (2023), “Smoothed quantile regression with large-scale inference,” *Journal of Econometrics*, 232, 367–388.
- Huang, C., Deng, Y., Yang, X., Cao, J., and Yang, X. (2021), “A network perspective of comovement and structural change: evidence from the Chinese stock market,” *International Review of Financial Analysis*, 76, 101782.
- Ji, P. and Jin, J. (2016), “Coauthorship and citation networks for statisticians,” *The Annals of Applied Statistics*, 10, 1779–1812.
- Kaminsky, G., Lyons, R., and Schmukler, S. (2001), *Mutual Fund Investment in Emerging Markets: An Overview*, vol. 15, Springer.
- Kato, K., Galvao Jr, A. F., and Montes-Rojas, G. V. (2012), “Asymptotics for panel quantile regression models with individual effects,” *Journal of Econometrics*, 170, 76–91.
- Ke, Z. T., Fan, J., and Wu, Y. (2015), “Homogeneity pursuit,” *Journal of the American Statistical Association*, 110, 175–194.
- Ke, Z. T. and Jin, J. (2023), “Special invited paper: The SCORE normalization, especially for heterogeneous network and text data,” *Stat*, 12, e545.
- Koenker, R. and Bassett, G. (1978), “Regression quantiles,” *Econometrica: Journal of the Econometric Society*, 46, 33–50.
- Koenker, R. and Xiao, Z. (2006), “Quantile autoregression,” *Journal of the American Statistical Association*, 101, 980–990.

- Lamarche, C. (2010), “Robust penalized quantile regression estimation for panel data,” *Journal of Econometrics*, 157, 396–408.
- Li, J., Ren, D., Feng, X., and Zhang, Y. (2016), “Network of listed companies based on common shareholders and the prediction of market volatility,” *Physica A: Statistical Mechanics and its Applications*, 462, 508–521.
- Liu, R., Shang, Z., Zhang, Y., and Zhou, Q. (2020), “Identification and estimation in panel models with overspecified number of groups,” *Journal of Econometrics*, 215, 574–590.
- Rohe, K., Qin, T., and Yu, B. (2016), “Co-clustering directed graphs to discover asymmetries and directional communities,” *Proceedings of the National Academy of Sciences*, 113, 12679–12684.
- Schütze, H., Manning, C. D., and Raghavan, P. (2008), *Introduction to information retrieval*, vol. 39, Cambridge University Press Cambridge.
- Su, L., Shi, Z., and Phillips, P. C. (2016), “Identifying latent structures in panel data,” *Econometrica*, 84, 2215–2264.
- Wang, D. and Tsay, R. S. (2023), “Rate-optimal robust estimation of high-dimensional vector autoregressive models,” *The Annals of Statistics*, 51, 846–877.
- Wong, K. C., Li, Z., and Tewari, A. (2020), “Lasso guarantees for β -mixing heavy-tailed time series,” *The Annals of Statistics*, 48, 1124–1142.
- Wu, Y., Lan, W., Zou, T., and Tsai, C.-L. (2022), “Inward and Outward Network Influence Analysis,” *Journal of Business & Economic Statistics*, 40, 1617–1628.
- Xu, X., Wang, W., Shin, Y., and Zheng, C. (2022), “Dynamic network quantile regression model,” *Journal of Business & Economic Statistics*, 0, 1–15.

- Zhang, X., Wang, D., Lian, H., and Li, G. (2023), “Nonparametric quantile regression for homogeneity pursuit in panel data models,” *Journal of Business & Economic Statistics*, 41, 1238–1250.
- Zhang, Y., Wang, H. J., and Zhu, Z. (2019), “Quantile-regression-based clustering for panel data,” *Journal of Econometrics*, 213, 54–67.
- Zhu, Q., Tan, S., Zheng, Y., and Li, G. (2023a), “Quantile autoregressive conditional heteroscedasticity,” *arXiv preprint arXiv:2306.08794*.
- Zhu, X., Chang, X., Li, R., and Wang, H. (2019a), “Portal nodes screening for large scale social networks,” *Journal of Econometrics*, 209, 145–157.
- Zhu, X., Wang, W., Wang, H., and Härdle, W. K. (2019b), “Network quantile autoregression,” *Journal of Econometrics*, 212, 345–358.
- Zhu, X., Xu, G., and Fan, J. (2023b), “Simultaneous estimation and group identification for network vector autoregressive model with heterogeneous nodes,” *Journal of Econometrics*, 105564.